catalysts

MDPI

Review

The Power of Non-Hydrolytic Sol-Gel Chemistry: A Review

Ales Styskalik [1,2,3,*], David Skoda [4], Craig E. Barnes [3] and Jiri Pinkas [1,2]

1 Department of Chemistry, Masaryk University, Kotlarska 2, CZ-61137 Brno, Czech Republic; jpinkas@chemi.muni.cz
2 CEITEC MU, Masaryk University, Kamenice 5, CZ-62500 Brno, Czech Republic
3 Department of Chemistry, University of Tennessee, Knoxville, TN 37996-1600, USA; cebarnes@utk.edu
4 Centre of Polymer Systems, Tomas Bata University in Zlin, Tr. T. Bati 5678, CZ-76001 Zlin, Czech Republic; dskoda@cps.utb.cz
* Correspondence: 211138@mail.muni.cz; Tel.: +42-054-949-6493

Academic Editor: Damien P. Debecker
Received: 13 April 2017; Accepted: 18 May 2017; Published: 25 May 2017

Abstract: This review is devoted to non-hydrolytic sol-gel chemistry. During the last 25 years, non-hydrolytic sol-gel (NHSG) techniques were found to be attractive and versatile methods for the preparation of oxide materials. Compared to conventional hydrolytic approaches, the NHSG route allows reaction control at the atomic scale resulting in homogeneous and well defined products. Due to these features and the ability to design specific materials, the products of NHSG reactions have been used in many fields of application. The aim of this review is to present an overview of NHSG research in recent years with an emphasis on the syntheses of mixed oxides, silicates and phosphates. The first part of the review highlights well known condensation reactions with some deeper insights into their mechanism and also presents novel condensation reactions established in NHSG chemistry in recent years. In the second section we discuss porosity control and novel compositions of selected materials. In the last part, the applications of NHSG derived materials as heterogeneous catalysts and supports, luminescent materials and electrode materials in Li-ion batteries are described.

Keywords: non-hydrolytic; sol-gel; non-aqueous; metal oxides; porosity

1. Introduction

1.1. General Introduction

Sol-gel chemistry based on hydrolysis and condensation of metal alkoxides is a powerful and well-established technique used for the preparation of metal oxides in various forms—xerogels, aerogels, micro/nanoparticles, fibers, thin films, etc. The behavior of mixtures of metal alkoxides with alcohols and water, in reactions providing oxide materials, was first studied in the 19th century. The true boom of this research area, however, started between 1950 and 1980 and it continues to grow rapidly. The main advantage of this method is that it provides homogeneous and porous oxides by low temperature processing. Moreover, these substances are accessible in various forms and compositions. Therefore, the materials resulting from sol-gel chemistry have been applied in numerous applications—such as heterogeneous catalysts, protective coatings, optical materials, etc. [1–5].

Sol-gel chemistry also has disadvantages. In many cases the hydrolysis rates of metal alkoxides differ significantly (e.g., $Si(OR)_4$ vs. $Ti(OR)_4$ or $Si(OR)_4$ vs. $R'_xSi(OR)_{4-x}$. This disparity in reaction rates is an obstacle in the preparation of homogeneous mixed metal oxides and in the introduction of organic groups into the oxide materials. Phase separation occurs instead. Moreover, water during the drying of the gels can exert significant capillary forces leading to pore collapse. Materials resulting

from aqueous solutions are therefore usually microporous. Many procedures overcoming these issues have been described in the literature [6–10].

One possible and fundamental improvement is to switch to non-aqueous conditions and use oxygen donors other than water. A French group led by Corriu, Vioux, and Mutin extended pioneering studies [11–13] in this area and started back in the 1990s to study thoroughly procedures based on the condensation of metal chlorides with metal alkoxides for the synthesis of metal oxides. The alkoxide was in this case the oxygen donor, no water was used throughout the synthesis. The reaction rates leveled off and highly homogeneous dispersions of metal cations in mixed oxides were achieved. Moreover, volatile organic solvents were easily removed and thus product drying was streamlined. The resulting materials were mesoporous with surface areas as high as 1000 $m^2 \cdot g^{-1}$. Another advantage of this method was its simplicity [6,14,15].

Many other condensation routes excluding water have been developed since that time. Various precursors have been used as oxygen donors—ethers, alcohols, carboxylates, carboxylic acids, etc. The name for this research area was coined as non-hydrolytic sol-gel chemistry (NHSG) and it was shown to be advantageous in many ways as already reviewed. Easy access to highly homogeneous and porous mixed metal oxides was already mentioned [6,14,15], however NHSG proved to be particularly useful in the synthesis of crystalline metal oxide nanoparticles (NPs) as well. Here the atomic dispersion plays a key role again because highly homogeneous samples crystallize at lower temperatures. Processing of metal oxide NPs can be done in variety of non-aqueous solvents thus broadening the possibilities of NHSG chemistry [16–23]. Non-aqueous conditions are also useful in the synthesis of hybrid materials, where the homogeneous distribution of organic groups is achieved [24]. Another advantage is that more controllable conditions can provide uniform and stable siloxane polymers [25,26]. The condensation rates in NHSG are generally lower in comparison to hydrolytic sol-gel (HSG) which can be advantageous in the synthesis of oligomeric species as well. These can be used as building blocks in further materials processing [27–30]. So-called building block approach has paved the way to nanostructured materials with well-defined properties such as porosity and structure [31–33]. Last but not least non-aqueous chemistry has also found application in atomic layer deposition (ALD) [34–36].

NHSG reactions are usually slower and thus easier to control than HSG syntheses. The low-mass volatile condensation product is usually an organic compound. These two facts suggest that these reactions can be followed by infrared spectroscopy (IR), nuclear magnetic resonance (NMR), and gas chromatography coupled with mass spectrometry (GC-MS), or just by simple gravimetry where the mass of the eliminated compound determines the degree of condensation. In fact, many authors have taken advantage of NHSG chemistry and performed detailed studies which have provided valuable insights into the formation of various metal oxides [33,37–40]. One of the best examples was presented by Bilecka et al., who was able to correlate the decreasing concentration of precursor with ZnO NPs growth and determine the rate constants for particle growth [40].

Research described in recent publications (2013–2016) has shown that NHSG chemistry has been developing in many directions. There are new NHSG synthetic routes, new materials and finally new applications. This review is organized along these lines.

While recent NHSG reviews have focused mainly on the two most important NHSG syntheses (alkyl halide and benzyl alcohol route), we describe here some of the newer and developing synthetic pathways. These are described in the first part of the review (**Development of condensation routes**), compared with the two well-known routes, and their advantages are highlighted. The second part of the review is devoted to the tailoring of properties and focuses on **porosity** and **new compositions** (**New materials**). These two characteristics are very important in the area of catalysis and therefore we devote special attention to them. Finally, the third part (**New applications**) shows some contemporary examples of utilization of materials prepared by NHSG techniques.

1.2. Overview of Known Reaction Pathways

Alkyl halide elimination is a well-established NHSG method. It is a reaction between metal chloride and metal alkoxide (Equation (1)). Condensation and formation of M–O–M bonds gives rise to inorganic oxides, while volatile alkylchlorides are released as the organic products of the reaction. Alkyl halide elimination is a valuable one-step process that provides us with highly porous (mixed) metal oxides. The homogeneity of mixing at the atomic level is usually very high. The metal alkoxide group can be formed in situ by reaction of metal chloride with ether (Equation (2)) or primary/secondary alcohols (Equation (3)). Therefore, there are three subtypes of alkyl halide elimination reactions distinguished by the oxygen donor used: alkoxide, ether or alcohol [6,14,15].

$$\equiv\text{M–Cl} + \text{R–O–M}\equiv \rightarrow \equiv\text{M–O–M}\equiv + \text{RCl} \quad (1)$$

$$\equiv\text{M–Cl} + \text{ROR} \rightarrow \equiv\text{M–O–R} + \text{RCl} \quad (2)$$

$$\equiv\text{M–Cl} + \text{ROH} \rightarrow \equiv\text{M–O–R} + \text{HCl} \quad (3)$$

Reactions of chlorosilanes with dimethylsulfoxide (DMSO) present a small branch of alkyl halide elimination. DMSO works here as an oxygen source. The reaction between metal chlorides and DMSO is rather slow and therefore can be well-controlled and offers interesting products such as cage siloxanes [27,30].

The reactivity of tertiary alcohols and benzyl alcohol toward the metal chlorides differs from primary and secondary alcohols. This reaction leads to the formation of M–OH groups and benzyl chloride (Equation (4)). Hydroxy groups consequently condense with M–Cl groups (Equation (5)) and form inorganic oxides. In this case it was found that reactions of metal chlorides with benzyl alcohol at temperatures between 180 and 250 °C provide crystalline metal oxide nanoparticles (compare with amorphous and porous products in the previous case). This method developed rapidly into the well-known **benzyl alcohol route**, and other compounds were soon identified as suitable metal oxide precursors (alkoxides, acetylacetonates, acetates). It provides monodisperse nanoparticles without any added surfactant. Benzyl alcohol works effectively as a solvent, an oxygen source, and a capping agent [16–22].

$$\equiv\text{M–Cl} + \text{C}_6\text{H}_5\text{CH}_2\text{OH} \rightarrow \equiv\text{M–OH} + \text{C}_6\text{H}_5\text{CH}_2\text{Cl} \quad (4)$$

$$\equiv\text{M–OH} + \text{Cl–M}\equiv \rightarrow \equiv\text{M–O–M}\equiv + \text{HCl} \quad (5)$$

Thermal decomposition of metal *tris*(^{t}butoxy)siloxydes (Equation (6)) is another well-known method for the preparation of amorphous and porous mixed metal oxides. The beneficial influence of templates on porosity under NHSG conditions has been demonstrated in this case [41].

$$\text{M(OSi(O}^t\text{Bu)}_3)_x \rightarrow \text{MO}_{x/2}\cdot x\text{SiO}_2 + 3x\ \text{CH}_2{=}\text{CMe}_2 + 1.5x\ \text{H}_2\text{O} \quad (6)$$

Ester elimination (Equation (7)) is the reaction between metal alkoxides and acetates. It was studied in the 1950s by Bradley as a route to metal trimethylsilyloxides [42], and later in the 1990s as a synthetic pathway to mixed metal oxo-clusters [43,44] and oxides [45,46]. However, it has been used only rarely and with limited success since then. Recently, it was discovered that acetoxysilanes react with trimethylsilyl esters of phosphoric and phosphonic acids in similar way providing highly homogeneous silicophosphates and acetic acid esters as organic products [39]. Mild reaction conditions have yielded a broad variety of hybrid derivatives [47].

$$\equiv\text{M–O–R} + \equiv\text{M–OC(O)R}' \rightarrow \equiv\text{M–O–M}\equiv + \text{RC(O)OR}' \quad (7)$$

A new way to highly porous and homogeneous metallosilicates was described recently as the **acetamide elimination** route. Reactions of acetoxysilanes with metal amides provide a high number

of M–O–M bonds and dialkylacetamide as a volatile organic product (Equation (8)). The advantages of templating were fully exploited in this synthetic procedure [38,48–51].

$$\equiv M–NR_2 + \equiv M–OC(O)R' \rightarrow \equiv M–O–M\equiv + R'C(O)NR_2 \quad (8)$$

Piers-Rubinsztajn reaction (or dehydrocarbon condensation) is the reaction between silanes and silicon alkoxides giving rise to Si–O–Si bonds and an alkane (Equation (9)). It is catalyzed by *tris*(pentafluorophenyl)borane and utilized mainly in the synthesis of siloxane polymers, but its application to the preparation of hybrid mixed oxide (Si–O–B) systems was shown recently [25,26,52–54].

$$\equiv M–H + R–O–M\equiv \rightarrow \equiv M–O–M\equiv + RH \quad (9)$$

Two molecules of metal alkoxides condense together during the **ether elimination** reactions (Equation (10)). These were studied already by Bradley in the 1950s and were used only in few cases (mainly with alkoxides of Mo^{VI}, W^{VI}, and Nb^{V}) [55]. A new application was recently found in the synthesis of mixed metal oxide nanoparticles [56,57].

$$\equiv M–O–R + R–O–M\equiv \rightarrow \equiv M–O–M\equiv + ROR \quad (10)$$

2. Development of Condensation Routes

2.1. Mechanistic View into Alkyl Halide Elimination, Implications for Homogeneity

The alkyl halide elimination reaction is used for the preparation of a wide variety of products including mixed metal oxides. At first glance, this reaction in principle seems to be very versatile, however closer inspection reveals different behaviors for various precursors which impacts particularly the product properties. It is useful to be aware of these differences and we wish to highlight some of them in this part of the review. Although we cite here mainly relatively old literature (1990–2000), it provides a good background for NHSG mixed metal oxide syntheses.

Redistribution reactions (ligand exchange, scrambling, metathesis) occur between metal halides and alkoxides prior to condensation in all cases (Equation (11)) [58]. These are the fastest reactions that are observed, occurring immediately after precursor mixing in alkyl halide elimination. Metal chloroalkoxides are therefore the true precursors in this NHSG condensation. As a result, mixing of $\mathbf{M}Cl_x$ with $\mathbf{M'}(OR)_y$ or $\mathbf{M}(OR)_x$ with $\mathbf{M'}Cl_y$ usually makes no difference. The properties (homogeneity, texture, etc.) depend strongly on the kinetics of hetero- (Equation (12)) vs. homocondensation (Equation (13)) [58].

$$\mathbf{M}Cl_x + \mathbf{M'}(OR)_y \rightarrow \mathbf{M}(Cl)_{x-z}(OR)_z + \mathbf{M'}Cl_z(OR)_{y-z} \quad (11)$$

$$\equiv \mathbf{M}–Cl + R–O–\mathbf{M'}\equiv \rightarrow \equiv \mathbf{M}–O–\mathbf{M'}\equiv + RCl \quad (12)$$

$$\equiv \mathbf{M}–Cl + R–O–\mathbf{M}\equiv \rightarrow \equiv \mathbf{M}–O–\mathbf{M}\equiv + RCl \quad (13)$$

Highly homogeneous networks can be produced only if the rate of heterocondensation of **M** and **M´** (Equation (12)) is at least comparable or higher than that of homocondensation (Equation (13)) [58]. Indeed, the kinetics of the hetero- vs. homocondensation reactions depend strongly on the nature of metal precursors and therefore the homogeneity of the products (described mainly on the basis of crystallization behavior and solid-state NMR studies) varies from case to case. Thus, it was shown, that Al–O–Ti system offers highly homogeneous products, which formed a metastable pseudo-brookite β-Al_2TiO_5 phase during the calcination [59,60]. Similarly, many other systems were shown to produce highly homogeneous materials, as well as new and metastable phases (e.g., $ZrTiO_4$ [61], $M_2Mo_3O_{12}$ (M = Ga, Y, Sc, Fe, In, Al)) [62–65]. High homogeneity was described in the Al–O–Si [66] and Zr–O–Si [67] mixed oxides as well. On the other hand, the incorporation of Ti into the silicate matrix was shown to be limited to ca. 9% [67] and was rationalized on the basis of thermodynamic instability of dispersed titanium in silicate matrices at higher Ti loadings [68]. Finally, an abrupt decrease in homogeneity was

observed in the case of organosilsesquioxane-metal oxide hybrids. Reactions of $MeSiCl_3$ with $AlCl_3$ in the presence of diisopropylether displayed only a limited formation of Si–O–Al bridges, and if $TiCl_4$ or $ZrCl_4$ were reacted with $MeSiCl_3$ and diisopropylether, no Si–O–M bonds were observed in the ^{29}Si cross-polarization magic angle spinning (CPMAS) NMR spectra [69]. High homogeneity in this type of hybrid material was later achieved when $MeSiCl_3$ or Me_3SiCl were used along with $SiCl_4$ and reacted with $TiCl_4$ and diisopropylether [70].

Several side reactions have been reported for the alkyl halide elimination and again their occurrence depends strongly on the nature of the metals used in the reaction system. For example, formation of hydrocarbons was observed during the synthesis of TiO_2 from $TiCl_4/Ti(O^iPr)_4$ and $TiCl_4/{}^iPr_2O$ mixtures. This was explained by possible dehydrochlorination of organic by-product, isopropylchloride, leading to alkene formation which can subsequently oligomerize to longer hydrocarbons [71]. Dehydrochlorination as well as alkene oligomerization reactions are known to be catalyzed by Lewis acids and thus feasible under the given conditions. The occurrence of these reaction by-products was also observed in the synthesis of zirconia NPs, which was performed at 340 °C [72]. Other reports of high temperature (>300 °C) alkyl halide condensations frequently do not examine the volatile products and therefore the occurrence of such side reactions is not known [73–77].

Another example of variability may be seen in the synthetic study of D/Q siloxane resins by alkyl halide elimination [78]. The reaction between Me_2SiCl_2, $Me_2Si(OMe)_2$, $SiCl_4$, and $Si(OMe)_4$ produced not only the expected MeCl, but also MeOMe as a by-product. The condensation reaction was catalyzed by Lewis acidic metal chlorides and the extensive study showed significant differences in the behavior of these catalysts. While $ZrCl_4$ and $TiCl_4$ were found to be highly selective catalysts for MeCl elimination, a significant production of dimethylether was observed in the reactions catalyzed by $FeCl_3$ and $AlCl_3$ [78].

Other examples of variability in alkyl halide elimination reactions depend on the route chosen. Let us focus on the "alkoxide route" (with metal chlorides and alkoxides as precursors, Equation (1)) and "ether route" (with metal chlorides and ethers as precursors; the alkoxide group is formed in situ, Equation (2)) [66]. The "alcohol route" is somewhat different and will be discussed later (Section 2.7). It was reported that the alkoxide and ether routes provide products with different degree of condensation, time of gelation, and porosity (Figure 1) [79]. The $TiCl_4/Ti(O^iPr)_4$ and $TiCl_4/{}^iPr_2O$ system was studied in detail by the NMR spectroscopy in solution in order to understand the reaction paths [37].

As already discussed, mixing of $TiCl_4$ and $Ti(OR)_4$ at r.t. leads very quickly to the equilibrium mixture of $TiCl_x(OR)_{4-x}$, with x depending on the Cl:OR ratio. In contrast, the condensation of organic groups to form Ti–O–Ti bridges, and elimination of RCl is much slower and takes place only at increased temperatures [37]. The most reactive species (probably catalyst which enhances condensation) was identified as $TiCl_3(OR)$. Thus it was shown that reaction mixtures with excess of $TiCl_4$ condense rapidly, while the inverse stoichiometric ratio provides relatively stable solutions of titanium chloroalkoxides with only a limited number or Ti–O–Ti bridges formed [37].

In the "ether route" the first reaction between $TiCl_4$ and diisopropylether is the coordination of ether to Ti followed by formation of $TiCl_3(O^iPr)$ and ${}^iPrCl$. The next exchange of the second Cl with an isopropoxy group is much slower and the content of $TiCl_3(O^iPr)$ is much higher in comparison to alkoxide route (1:1 ratio). As noted above, this complex was identified as the most reactive species and therefore the condensation starts more rapidly in comparison to the alkoxide route. This leads to shorter gelation times and higher degrees of condensation, with the texture of the resulting product being influenced as well [37].

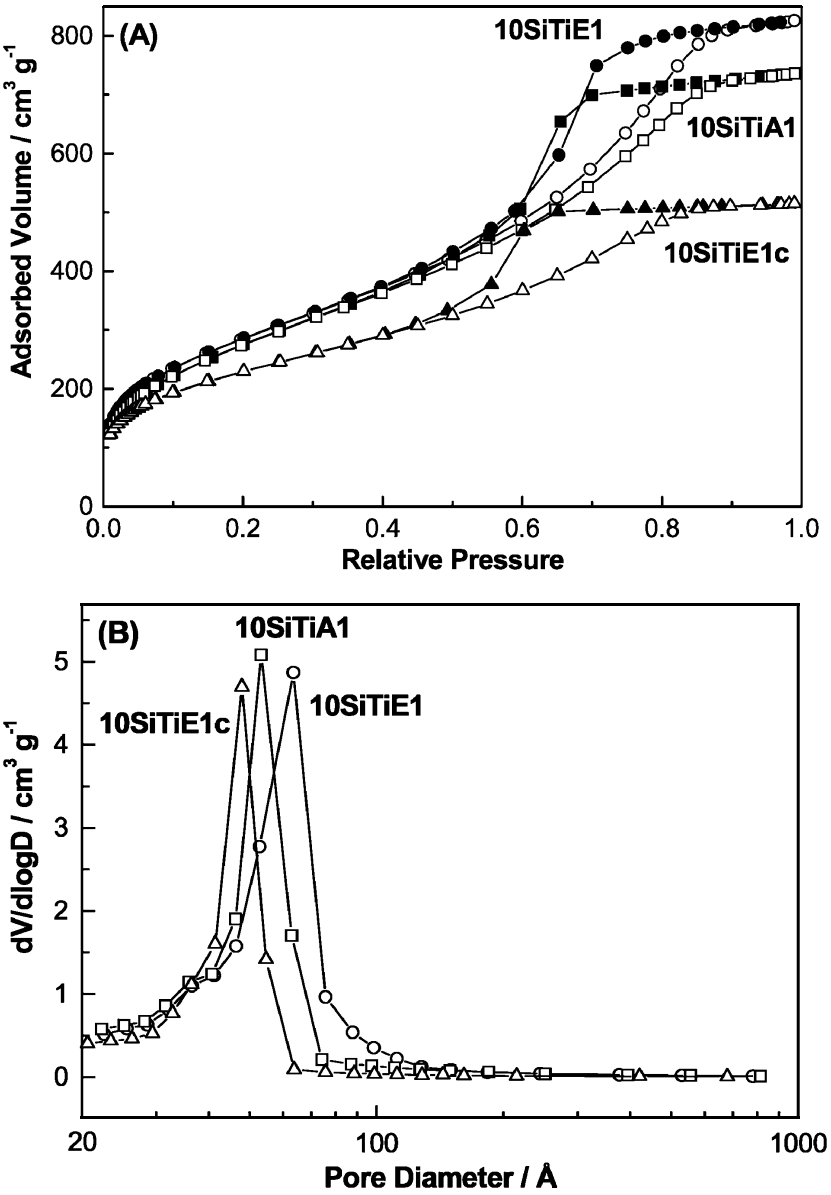

Figure 1. N_2 physisorption results at 77 K of "standard" xerogels prepared by the alkoxide route (10SiTiA1) or by the ether route (10SiTiE1), and of 10SiTiE1 calcined in air at 500 °C for 5 h (10SiTiE1c). (**A**) Adsorption-desorption isotherms (open and filled symbols correspond to the adsorption and desorption branches, respectively); (**B**) pore size distributions derived from the desorption branches, using the BJH method. Reproduced with permission from [79]. Copyright American Chemical Society, 2004.

Diisopropylether was identified in other mixed oxide syntheses as ideally suited for alkyl halide elimination in the ether route. It forms a relatively stable carbocation and this feature facilitates condensation reactions. Use of diisopropylether as an oxygen donor therefore led to short gelation times and high degrees of condensation [61]. Moreover, the synthetic work-up is very simple, uses readily available metal chlorides and ether (no need for alkoxides), and yields high surface area materials. There are neither restrictions limiting compositions, nor were negative effects observed on homogeneity in mixed metal oxide synthesis [59,61,66,67,80]. For these reasons, the ether route is currently the most widely used for the preparation of mixed metal oxides in the NHSG community.

2.2. High Homogeneity of Mixed Metal Oxides in Acetamide Elimination

The acetamide elimination was recently introduced as a new condensation reaction of metal amides with silicon acetates (Scheme 1) and used for the synthesis of metallosilicates (M = Ti, Zr, Al, Sn) [38,48–51]. Importantly the acetamide elimination was shown to provide materials of high homogeneity and high Si–O–M content. This was confirmed by IR and MAS NMR spectroscopy as well as by crystallization studies. The direct comparison of materials prepared by alkyl halide and acetamide elimination routes in terms of homogeneity is possible for Si–O–Al, Si–O–Zr, and Si–O–Ti systems.

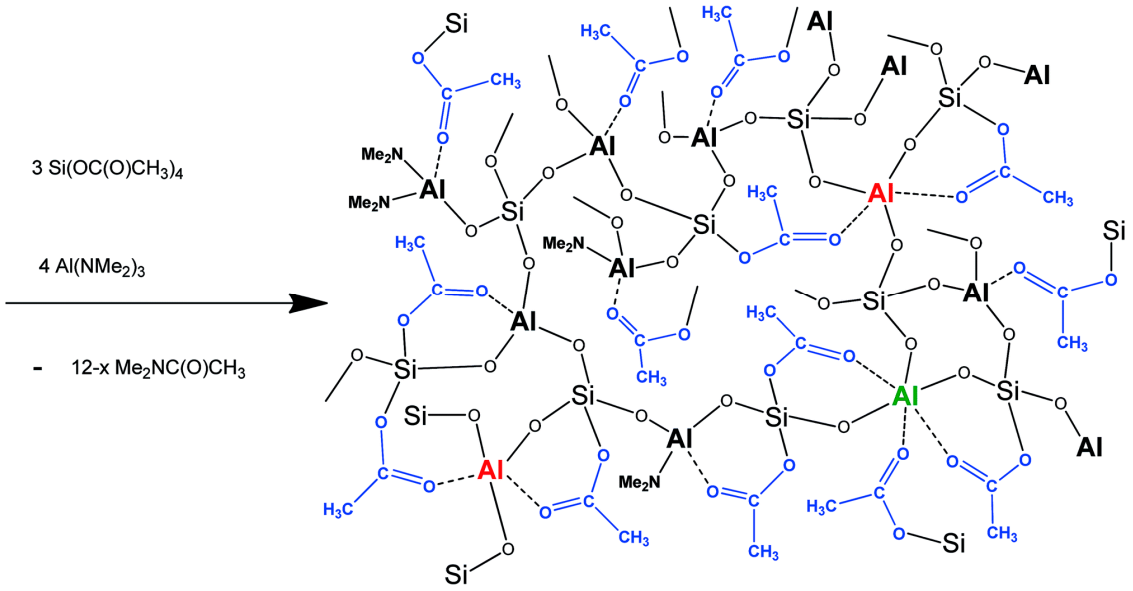

Scheme 1. Synthesis of aluminosilicate gel with four-, five-, and six-coordinate Al atoms and residual acetate and dimethylamide groups. Reproduced with permission from [51]. Copyright Royal Society of Chemistry, 2016.

Lowfield ^{29}Si CPMAS NMR resonances signal the formation of Si–O–M bridges and serve as a commonly used benchmark for the high homogeneity of metallosilicates (Figure 2). Similar lowfield shifts were reported for samples coming from both acetamide and alkyl halide elimination. The only striking difference was observed in the case of organosilsesquioxane-metal oxide hybrids. While reactions of $MeSiCl_3$ with $AlCl_3$ in the presence of diisopropylether provided materials with only limited amount of the Si–O–Al bridges as evidenced by an intense signal at −66 ppm ($MeSi(OSi)_3$ groups) and a resonance of low intensity at −47 ppm ($MeSi(OAl)_3$ groups), condensation of $(AcO)_3Si–CH_2CH_2–Si(OAc)_3$ with $Al(NMe_2)_3$ afforded highly homogeneous products featuring a broad composite signal in the ^{29}Si CPMAS NMR spectra corresponding to $CH_2Si(OSi)_{3-x}(OAl)_x$ (x = 0–3) moieties.

In the case of aluminosilicates, both methods give rise to early crystallization to form mullite [51,66]. In the case of zirconosilicates, using a 1:1 Zr:Si ratio, the crystallization of ZrO_2 takes place at 600 °C and $ZrSiO_4$ is observed only after calcination at 1500 °C in the products of alkyl halide elimination [67], while the samples from acetamide route remain amorphous up to 850 °C and their crystallization to zircon occurs at the temperatures as low as 1100 °C [50]. Early zircon crystallization points to high homogeneity at the atomic scale. More elaborate procedures (e.g., mineralization, usage of nanoparticles or zircon seeds, etc.) are necessary to achieve such low crystallization temperatures [81–83]. In the case of titanosilicates (in Si:Ti 1:1 ratio) phase separation and crystallization of anatase was observed at higher temperatures for acetamide samples (600 or 800 °C depending on heating ramp) [38,48] in comparison to alkyl halide samples (500 °C) [67]. Bearing in mind that the crystallization temperatures

are influenced by properties other than homogeneity (e.g., particle size, sample amount, heating ramp, etc.) these data suggest that the homogeneity could be improved in the case of acetamide elimination at least in these particular examples.

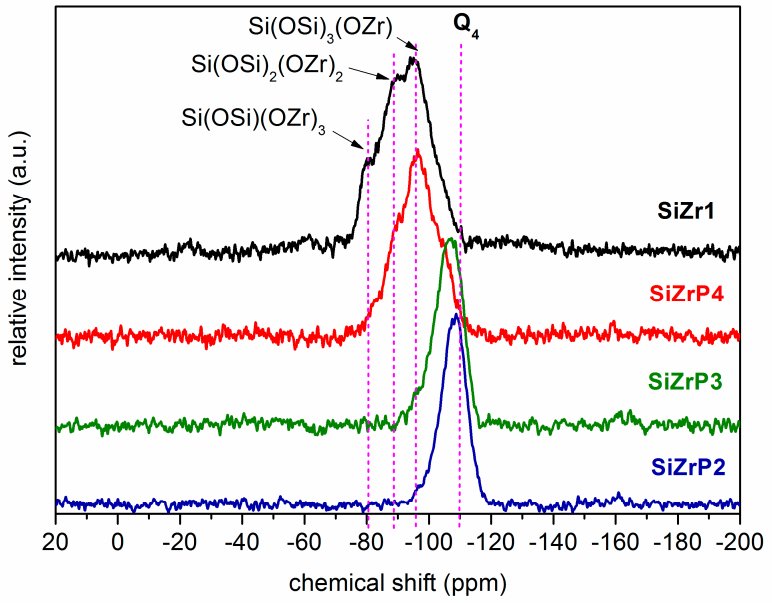

Figure 2. ^{29}Si CPMAS NMR spectra of dried zirconium silicate xerogels. Reproduced with permission from [50]. Copyright Springer, 2015.

While it is hard to identify all the reasons for these differences, there are some common features observed for these methods and others in which they differ. There is no doubt that the redistribution reaction followed by homocondensation takes place in acetamide systems as a side reaction to heterocondensation similar to mixtures of metal chlorides and alkoxides. Si–O–Si bridges are observed by IR and ^{29}Si CPMAS NMR spectroscopy in both cases. The most distinguishing feature for acetamide systems is the presence of bridging acetates—observed in the IR and ^{13}C CPMAS NMR spectra (Scheme 1). Coordination of acetates to metal centers is generally very fast in solution [84] and this has two consequences: (i) the initial structures based on Si–O–C(CH_3)=O→M bridges are formed very quickly (compare with the strategy used for the hydrolytic sol-gel preparation of homogeneous titanosilicates used by Flaig [7]) and (ii) the reactivity of metal amides is decreased and leveled to silicon acetates as the coordination number of highly oxophilic metal centers is increased by carbonyl oxygens. Calcination then leads to the elimination and oxidation of acetates, but importantly the homogeneity is preserved.

It should be noted that the surface areas and pore volumes of acetamide elimination samples were rather poor in comparison to metallosilicates coming from the alkyl halide route [38]. This was significantly improved with the use of block copolymer templates (Pluronic P123 and others), and highly porous materials were obtained [48–51]. The addition of these pore generating agents to the reaction mixtures led in turn to even better homogeneity, as suggested by crystallization behavior of the samples [48,50]. It can be argued that these polyethers work similarly to acetates—their oxygens coordinate to metal centers further decreasing their reactivity and leveling it to silicon acetates. Subsequent assembly during the condensation reactions results in three-dimensional systems consisting of the Si–O–M linkages and copolymer chains. This feature of acetamide elimination strongly resembles strategies used in the hydrolytic sol-gel method for improving homogeneity, where acetic acid or acetylacetone is added to the reaction mixtures, coordinates to metal centers, and decrease their high reactivity to the level of slow-hydrolyzing silicon alkoxides [7–10].

2.3. Building Block Approach to Single Site Metallosilicate Catalysts

Another example of achieving homogeneity on an atomic level involves a sequential addition strategy based on the reaction of a silicate building block ($Si_8O_{12}(OSnMe_3)_8$) with metal chlorides [85]. The silicate cube features a rigid and stable building block, which can be connected by spatially isolated metal centers. The reaction cleanly produces cross-linked metallosilicate networks and trimethyltinchloride (Equation (14)), no side or reversible reactions were observed. The final mesoporous material is formed after a second round of condensation with chlorosilanes (e.g., $SiCl_4$, Me_2SiCl_2, $HSiCl_3$, ...) which provide stable Si–O–Si bonds in the matrix (Equation (15)). The reaction resembles alkyl halide elimination; however, there are very significant differences between the two: (i) no ligand exchange of trimethyltin groups with chlorine substituents was observed and (ii) the Me_3Sn-moieties are much easier to eliminate than alkyl-groups and the precursors condense already at r.t. Owing to these important features this method allows for the preparation of dispersed metal centers in silicate matrix, or in other words single site metallosilicate catalysts.

$$Si_8O_{12}(OSnMe_3)_8 + MCl_x \rightarrow Si_8O_{12}(OSnMe_3)_7(–O–MCl_{x-1}) + Me_3SnCl \quad (14)$$

$$Si_8O_{12}(OSnMe_3)_8 + SiCl_4 \rightarrow Si_8O_{12}(OSnMe_3)_7(–O–SiCl_3) + Me_3SnCl \quad (15)$$

The ability of this procedure to provide us with single site metal centers was demonstrated in a detailed research study of reactions of vanadyl trichloride, $VOCl_3$, with the silicate building block ($Si_8O_{12}(OSnMe_3)_8$) [33]. Depending on the sequence of addition and molar ratios used, the authors were able to prepare 1-, 2-, and 3-connected samples (Scheme 2, $Cl_2V(O)(OSi\equiv)$, $ClV(O)(OSi\equiv)_2$, and $V(O)(OSi\equiv)_3$, respectively). The identity of these unique sites was evidenced by gravimetry (number of equivalents of Me_3SnCl eliminated during the reaction), ^{51}V solid-state NMR spectroscopy, XANES, and EXAFS analyses. Mainly the careful analyses of XANES and EXAFS data serve as strong evidence of successful synthesis of targeted single site vanadyl species within the silicate matrix. The conclusions were further supported by the ^{17}O solid-state NMR (both 1D and MQMAS) analyses of samples enriched with ^{17}O. Finally, it is important to note that this methodology is versatile and the condensation of trimethyltin silicate cube with a wide variety of metal chlorides ($SnCl_4$, $TiCl_4$, $ZrCl_4$, VCl_4) was recently suggested [86].

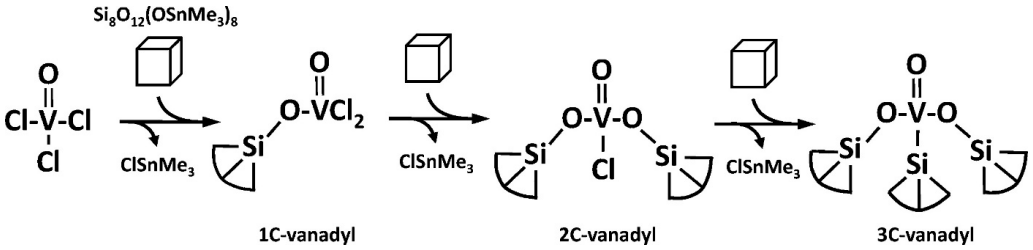

Scheme 2. The targeted synthesis of single site vanadyl species on the surface and in the framework of silicate building block materials. Reproduced with permission from [33]. Copyright Elsevier, 2011.

2.4. New Materials by Ester Elimination: Silicophosphates and Their Hybrid Derivatives

The ester elimination was studied similar to alkyl halide elimination back in the 1990s in the context of synthesizing homogeneous mixed metal oxides. The pioneering studies by Bradley et al. [42] were later complemented by mechanistic insights developed by J. Caruso and M. J. Hampden-Smith on the $Sn(O^tBu)_4$-$Sn(OAc)_4$, $Sn(O^tBu)_4$-Me_3SiOAc and $Sn(O^tBu)_4$-$Pb(OAc)_4$ systems. These authors identified criteria which avoid the ligand exchange: Use of (i) non-coordinating solvents; (ii) small carboxylate ligands; and (iii) an electropositive metal alkoxide [43,44,87,88]. A high homogeneity was achieved in the ternary Ba–O–Si–O–Ti system [46], however later attempts to use this strategy for Zr–O–Si [45] and Ti–O–Si [38,89] systems suffered significantly from the ligand exchange,

homocondensation and rather low homogeneity though the criteria suggested by Caruso and Hampden-Smith were followed. These problems may be overcome only if Ti is embedded in the starting precursor cubic μ-oxo Si–O–Ti complex which was probably preserved during its immobilization into the silica matrix [89]. Other less conventional transesterification pathways were used to prepare mixed oxides (e.g., reactions of $Si(OEt)_4$ with $(MeO)_3B_3O_3$ [90–92] and $Ti(NO_3)_4$ [93] producing $B(OEt)_3$ and $EtONO_2$, respectively, as volatile reaction products), however the homogeneity of these materials was not studied in these cases. The synthesis of mixed metal oxides by ester elimination is seldom used nowadays owing to these reasons. There are a few reports of the siloxane formation, which are described in Section 2.6, focusing on oligo- and polysiloxanes.

Ester elimination has, however, recently been used in the synthesis of highly homogeneous and porous silicophosphate materials from silicon acetates and trimethylsilyl esters of phosphoric and phosphonic acids (Scheme 3) [39,47,94,95]. Skeletal Si–O–P bonds in silicophoshates are prone to hydrolysis and therefore it is highly desirable to use anhydrous conditions during synthesis. This was achieved during non-hydrolytic ester elimination reactions. Neither ligand exchange nor homocondensation were observed in the reaction mixtures and high homogeneity at the atomic scale was attained. This was proved mainly by early crystallization of silicon phosphates and the ^{29}Si CPMAS NMR spectroscopy where a strong resonance assigned to $Si(OP)_6$ moieties was observed, with no evidence of Si–O–Si or P–O–P bond formation detected [39].

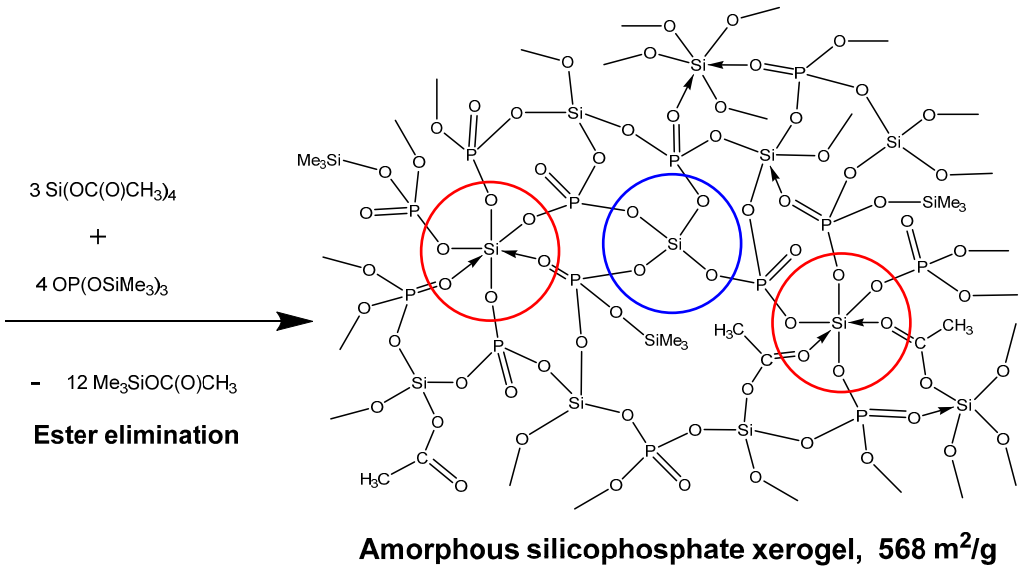

Scheme 3. Ester elimination reaction producing silicophosphate materials. Reproduced with permission from [39]. Copyright Elsevier, 2014.

It should be noted that the reactions of silicon acetates and trimethylsilyl esters of phosphoric and phosphonic acids differ significantly from the condensations between metal acetates and metal alkoxides. There are no electropositive metal centers present where carbonyl groups could attack. Instead there are easily eliminated Me_3SiO groups which facilitate the condensation (Scheme 3). The absence of reactive metal centers also prevents the ligand exchange from occurring. These are probably the main reasons which allow high homogeneity to be attained in this particular system.

Another important feature of this preparation is that the synthesis of hybrid derivatives was shown to be easily accessible. Both C–Si and C–P bonds were stable under the reaction conditions no matter whether alkyl or aryl groups were used [47]. While the homogeneity of Si–O–P mixing was preserved in these hybrid derivatives, the porosity [47] and hydrolytic stability [94] were influenced by the incorporation of organic groups. The control over porosity in hybrid silicophosphate materials will be described in more detail in Section 3.1.1.

There is one more completely different set of condensation reactions which is commonly referred to as ester elimination. The reaction mixtures are usually composed of metal alkoxides and carboxylic acids. The possible formation of hydroxy groups and water in situ causes this method to be similar to hydrolytic sol-gel condensations. In order to clearly distinguish between this method and truly non-hydrolytic ester elimination, this approach is presented in a separate part of the review (Section 2.5).

2.5. Carboxylic Acids in NHSG

The application of acetic acid in the sol-gel preparation of silica, thus avoiding water as a solvent and a reactant, was reported in 1994 [96]. The main advantage described there was the decrease of gelation time by two to three orders of magnitude. Carboxylic acids are currently used mainly in the synthesis of metal oxide nanoparticles, where they bind to the metal oxide surfaces and stabilize the nanoparticles. It should be noted, that hydroxy groups can be formed during this process and their condensation can lead to the in situ formation of water. Therefore, this method may be classified between HSG and NHSG and only a few inspiring examples of the application of carboxylic acids in NHSG methods will be cited here.

The use of acids during sol-gel condensations can have several advantages: (i) The acids can level reaction rates of different precursors by coordination to the metal centers and therefore could be used in the synthesis of mixed metal oxides for improving homogeneity [97–99]; (ii) Carboxylic acids are miscible with and soluble in a broader range of solvents than water because they combine hydrophobic tail and hydrophilic head. This was exploited in the templating of silica with ionic liquids which provided materials with excellent pore volumes and surface areas [100–104], in the large-scale synthesis of monodispersed bridged polysilsesquioxane nanoparticles [105], or when reacting metal precursors bearing bulky organic groups [106]; (iii) Carboxylates bind strongly to the metals and therefore could work as surfactants hindering further growth of particles. Monodispersed metal oxide nanoparticles have been prepared in this way [107–109].

A completely different and truly non-hydrolytic example of carboxylic acids in NHSG reactions was described in a very recent paper [110]. In this case acetic acid is released as the organic product of the condensation reaction between polyfunctional phenols and silicon tetraacetate (Scheme 4). The resulting amorphous aromatic organosilicates are highly porous (up to 990 $m^2 \cdot g^{-1}$ and 1.36 $cm^3 \cdot g^{-1}$) and their porosity can be controlled by careful choice of precursor. This method represents a novel NHSG synthetic route to materials which can be used as supports for heterogeneous catalysts or adsorbents.

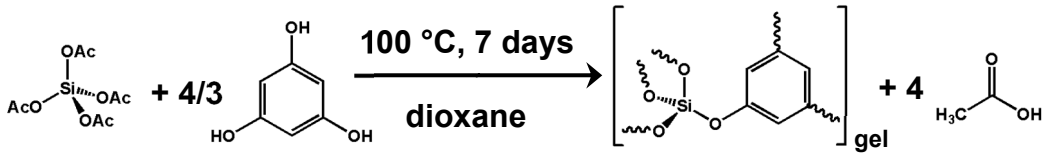

Scheme 4. Synthesis of highly porous aromatic organosilicates. Reproduced with permission from [110]. Copyright Elsevier, 2017.

2.6. Siloxanes by NHSG Condensations, Piers-Rubinsztajn Reaction

NHSG condensation strategies significantly impacted the synthesis of oligomers and polymers with backbone composed of Si–O–Si bonds—siloxanes [25,111]. Molecular siloxane compounds, linear siloxane polymers, and 3D siloxane (hyperbranched) polymers are representatives of this class of compounds. The aim here is not to give an exhaustive overview of research in this area, but to give readers an outline of the main features of this research. The knowledge of NHSG condensations gained in this research area could be usefully applied to the synthesis of mixed metal oxides and their hybrid derivatives and vice versa. Readers who wish to study the synthesis of oligo- and polysiloxanes more deeply are encouraged to consult the reviews focused on this particular topic [25,111].

The synthesis of oligo- and polysiloxanes is dominated by the HSG approach based on the hydrolysis and condensation of alkoxy- and chlorosilanes. Similar to the synthesis of mixed metal oxides, the hydrolytic route to siloxanes is hard to control and provides mixtures of cyclic and linear polymers. The synthesis of explicit molecular siloxanes by HSG is not selective and hard to achieve. Moreover, the incorporation of two or more different siloxane units into the polymer leads to random and often very heterogeneous distributions of these units throughout these materials owing to different electronic properties of Si centers (e.g., Me_2SiO_2 vs. Ph_2SiO_2 vs. SiO_4). Finally, the solubility and stability of siloxane polymers play an important role as well. The solubility of polysiloxanes synthesized by HSG method is usually limited to water and alcohols since they possess a large amount of hydrophilic Si–OH groups. In addition, these reactive groups can condense further causing only limited stability of polymer suspensions for longer time periods. The NHSG condensations have proven to be particularly useful in overcoming these disadvantages of the HSG route.

Alkyl halide elimination is an important synthetic route to siloxanes, mainly to 3D cross-linked polymers and explicit molecular compounds. The synthesis of 3D cross-linked polysiloxanes has been described by Vioux and coworkers [78,112], and Hay and Raval [113–115]. Redistribution reactions of alkoxy and chloro groups take place readily at r.t., while the condensation reactions occur at temperatures from 35 to 150 °C and were catalyzed by Lewis acidic metal chlorides, similar to the syntheses of metal oxides (Section 2.1). Ligand exchange reactions led to "random homogeneity", but not perfect alternation of different siloxane units. The homogeneity was further negatively influenced by other side reactions. Dialkylether was observed as a condensation product together with alkyl halide in some cases [78], and cleavage of the Si–C bonds was observed during the synthesis of phenylsilsesquioxanes in sealed ampoules [112] (these bonds were stable when the Schlenk vessel was opened to N_2 atmosphere allowing for the release of alkyl halide from the reaction mixture) [113]. In spite of these side reactions the homogeneity and stability of 3D cross-linked siloxanes prepared by alkyl halide elimination were still superior to the materials prepared by HSG syntheses [78].

More recently Kuroda and coworkers [28,31,116,117] reported synthesis of explicit molecular alkoxysiloxanes with various functional groups (e.g., $Si[OSiH(OMe)_2]_4$, Scheme 5) by alkyl halide elimination. A weak Lewis acid, $BiCl_3$, was used in this case as a catalyst and alkoxy groups providing stable carbocations (^{t}Bu– and Ph_2CH–) were utilized in order to facilitate the condensation and avoid ligand scrambling and other side reactions. These reaction conditions yielded the desired compounds in reasonably high yields after purification suggesting that the careful choice of catalyst and leaving group significantly suppressed the unwanted side reactions commonly observed during alkyl halide elimination. Alkoxysiloxanes with different functional groups (e.g., Si–OR, Si–H, Si–CH=CH, etc.) are suitable for a large variety of further reactions (both HSG and NHSG condensations [29,118], hydrosilylation, co-polymerization, etc.) and therefore are very useful building blocks for the synthesis of structured silica-based materials [119]. Importantly, it was shown that these precursors can be reacted selectively and in a controlled way [117,118].

Another modification of alkyl halide elimination is the reaction of chlorosilanes with dimethylsulfoxide (Scheme 6). DMSO works here as an oxygen donor (instead of ether or alkoxy group), and no catalyst is needed. This method led to the synthesis of hexamethylcyclotrisiloxane (D3, from Me_2SiCl_2 and 2 eq. of DMSO) [27], and hexasilsesquioxane (T6) cages (Scheme 6) [30] in appreciable yields. This method was used to prepare organosilsesquioxane particles (diameter 0.1–0.2 μm) as well [120]. It is worth noting, that the cyclic and cage siloxanes are part of an important class of compounds (models of resins, precursors to polysiloxanes) and their hydrolytic synthesis was in most cases unsuccessful or highly inefficient (depending on the organic groups attached to the Si atoms) [30].

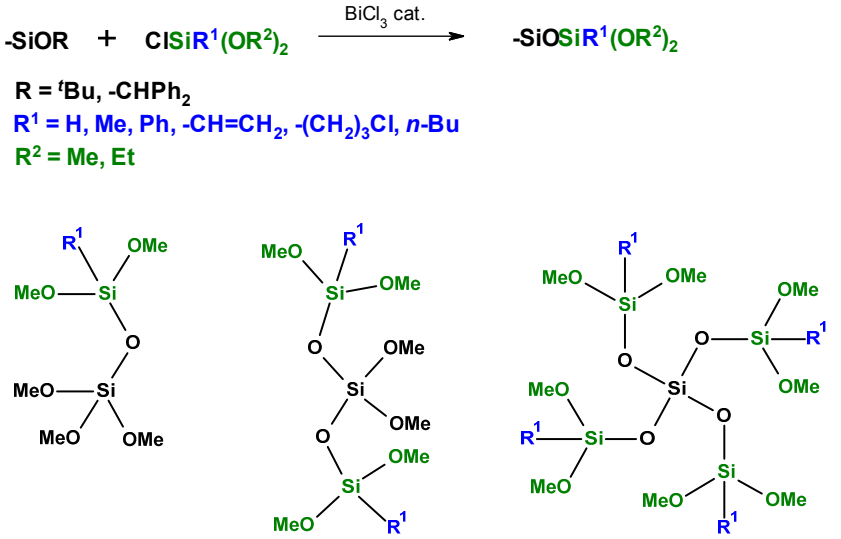

Scheme 5. Synthesis of discrete alkoxysiloxane oligomers by direct alkoxysilylation reaction. Reproduced with permission from [116]. Copyright Elsevier, 2012.

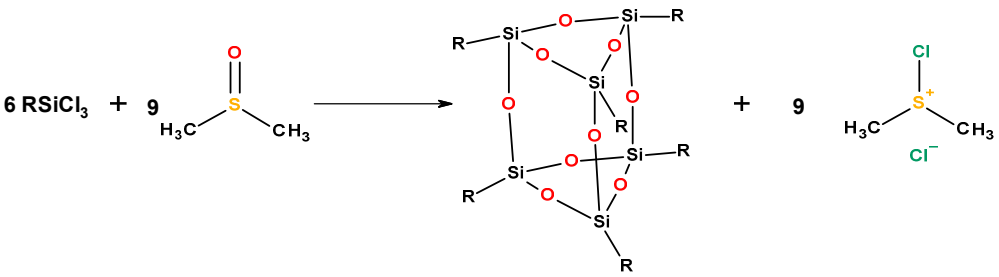

Scheme 6. Reaction of alkyltrichorosilane with DMSO producing hexasilsesquioxane cage. Reproduced with permission from [30]. Copyright Royal Society of Chemistry, 2003.

Ester elimination is a minor route, which was successfully applied to siloxane preparation [121,122]. The synthesis of stable 3D cross-linked siloxanes with a narrow distribution of molecular weights was reported starting from $Si(OEt)_4$ and acetic anhydride. The in situ formation of Si–OAc groups was catalyzed by $Ti(OSiMe_3)_4$ and ethylacetate was released as the volatile product of the condensation. The product of this reaction can be described as hyperbranched polyethoxysiloxane (no acetoxy groups are left after the synthesis), that is stable for long periods of time and soluble in organic solvents. It has a lower solubility in water and lower hydrolysis rates in comparison to tetraethoxysilane. Owing to these features, this polyethoxysiloxane was used as a precursor for the hydrolytic synthesis of silica membranes [123] and mesostructured silica particles [124–126].

Finally all three members of the siloxane family (molecular compounds [26,127], linear [128] and 3D cross-linked [53,129,130] polysiloxanes) were successfully prepared by the Piers-Rubinsztajn reaction (or dehydrocarbon condensation) as reviewed elsewhere [25,111]. Although research into this reaction type is strongly focused on the polymer science, the first examples of the preparation of porous silica-based hybrid materials [131] and mixed Si–O–B oxides [54] have been reported.

This strongly exothermic reaction is based on the condensation of Si–H and EtO–Si units (Scheme 7). Alkane is eliminated in the course of the reaction, which is catalyzed by the strong Lewis acid *tris*(pentafluorophenyl)borane, $B(C_6F_5)_3$. The catalyst plays an important role for hydride ion transfer [52,130]. Similar to the other NHSG syntheses, this reaction suffers from ligand exchange and homocondensation, which led to lower homogeneity in the final products. However, it can be strongly suppressed by a careful selection of starting compounds [26,128]. Thus it was shown by ^{29}Si NMR that

diphenyldimethoxysilane condenses with 1,4-*bis*(dimethylsilyl)benzene to produce almost perfectly alternating polymer, while a mixture of dimethyldimethoxysilane and 1,4-*bis*(dimethylsilyl)benzene is prone to ligand scrambling and only random homogeneity was achieved [128]. Significant differences in reactivity and tendency to ligand exchange were also observed when comparing tetramethoxysilane, tetraethoxysilane and *tetra*(isopropoxy)silane. This was explained by different steric hindrance at the Si atoms by the organic groups (Scheme 7) [26].

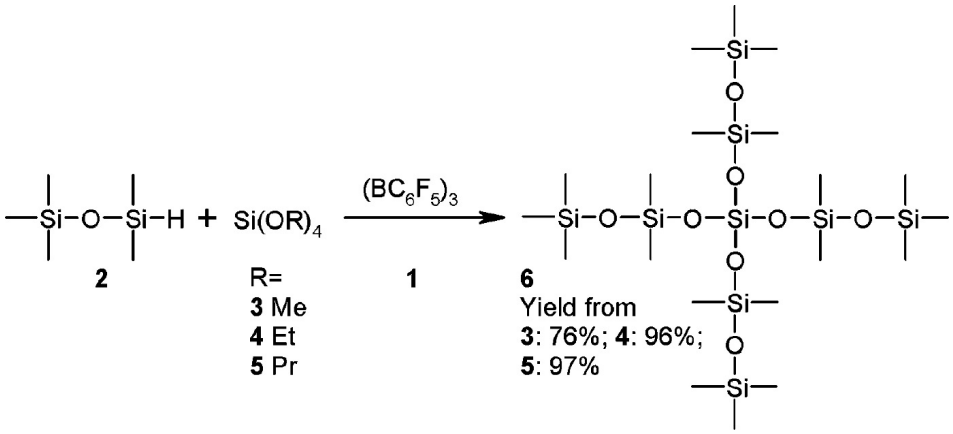

Scheme 7. Effect of steric environment on yield in synthesis of 6. Reproduced with permission from [26]. Copyright American Chemical Society, 2008.

The sequence of addition of precursors was suggested to play an important role as well [25]. Rubinsztajn and coworkers usually add the silanes dropwise to the solutions of alkoxysilanes and a catalyst in toluene. The ligand metathesis and homocondensation is observed mainly in the early stages of the reaction when alkoxysilane is in a large excess in comparison to the second reagent. As the reaction mixture gets closer to the desired stoichiometry, the heterocondensation starts to dominate the process [130]. In contrast, Brook and coworkers usually prepare a solution of starting precursors (silane + alkoxysilane) with desired stoichiometric ratios in hexane and then introduce the catalyst. In this way they were able to synthesize precise silicone compounds in high yields, suggesting that they were able to suppress the metathetic reactions (Scheme 7) [26,127].

2.7. Alcohols in NHSG

Alcohols as alternative non-aqueous solvents were used mainly in the alkyl halide elimination, where they played the role of oxygen donor as well. Their application is, however, reported significantly less often in comparison to alkoxides and ethers. Their reaction with metal chlorides leads to in situ formation of metal alkoxides and the release of HCl, which may catalyze secondary reactions leading to complex pathways. Therefore, these methods are somewhere between HSG and NHSG approach similar to the application of carboxylic acids in NHSG. However this method proved to be successful in the synthesis of amorphous mixed metal oxides [132–143]. Alcohols (and silanols) can also react with Si–H groups providing hybrid porous materials or building blocks based on Si–O–Si and Si–O–C bonds (condensation catalyzed by Et_2NOH) [117,144,145].

An example of alkyl halide elimination, alcohol route, was reported by Moravec et al. [146]. The reactions between dichloroethylalane, $EtAlCl_2$, and cyclohexanol, ^{n}butanol, phenol, and 2,4-di^{t}butylphenol at low temperatures yielded a wealth of various aluminum chloride alkoxides, eight of which were structurally characterized. These molecular compounds are precursors to materials based on Al_2O_3 obtained after the thermolysis of reaction mixture consisting of $EtAlCl_2$ and cyclohexanol at 150 °C. Cyclohexyl chloride was identified as volatile product. The resulting materials yielded poorly crystalline Al_2O_3 after calcination, surface areas reached up to 150 $m^2 \cdot g^{-1}$.

The performance of benzyl alcohol in alkyl halide elimination with its high boiling point, ability to form a stable carbocation and cap the surface of metal oxide particles led to a broad and fruitful research on the synthesis of crystalline metal oxide nanoparticles which is described in more detail in the next section (Section 2.8).

2.8. Benzyl Alcohol Route

The "benzyl alcohol route" developed by Niederberger and co-workers represents a versatile surfactant-free non-hydrolytic reaction system giving rise to numerous metal oxide nanoparticles and oxide-based inorganic–organic nanohybrids [16,19,22,147]. Metal precursors such as chlorides, alkoxides or acetylacetonates readily react with benzyl alcohol and subsequently form the corresponding oxide or mixed oxide nanoparticles. Depending on the precursor used, the reaction mechanism is proposed as alkyl halide or ether elimination. Recently, it was shown for the preparation of GeO_2 NPs that hydrolysis has to be considered as a potential pathway as well because water could be formed in situ [147]. The reaction parameters involve solvothermal treatment (e.g., 180–250 °C in the case of metal alkoxides). If the reactions are carried out in the presence of alkaline species, metal alkoxides react with benzyl alcohol by means of a C–C coupling mechanism [148]. This mechanism was described in the case of the non-aqueous formation of $BaTiO_3$ and $SrTiO_3$.

Benzyl alcohol—the organic solvent—also acts as a surfactant and provides the control of the nanoparticle shape, morphology and size distribution. However, the nature of precursor is important as well. For example, the reaction of niobium ethoxide in benzyl alcohol yields orthorhombic Nb_2O_5 particles with platelet-like morphologies and sizes ranging from 50 to 80 nm while the reaction of $NbCl_5$ in benzyl alcohol led to small, slightly agglomerated crystallites of just a few nanometers [149]. An interesting reaction was reported when yttrium isopropoxide was used as a precursor. The reaction with benzyl alcohol lead to a lamellar nanohybrid consisting of crystalline yttrium oxide layers with intercalated benzoate molecules [150]. Thus, it has been shown in numerous studies on the benzyl alcohol route that by choosing the appropriate reaction system, it is possible to gain control over the nanocrystal parameters.

Based on the development of new reaction techniques, the benzyl alcohol route was extended with the use of microwave reactor, which decreased the reaction times significantly and enabled scale-up of the syntheses to multi-gram quantities [20,40]. An interesting study reported by Bilecka et al. focused on the microwave assisted synthesis and kinetic analyses of ZnO nanoparticles from zinc acetate in benzyl alcohol. Compared to conventional heating, the microwave-assisted route greatly accelerated the formation of nanoparticles by: (i) facilitating the dissolution of a precursor in the solvent; (ii) increasing the rate of the esterification reaction, resulting in faster production of monomer and consequently earlier nucleation; and (iii) increasing the rate of crystal growth from 3.9 $nm^3 \cdot min^{-1}$ (conventional heating) to 15.4 $nm^3 \cdot min^{-1}$ (microwave heating) (Figure 3). A mechanism of ZnO nanoparticle formation was proposed based on the results of this work. The esterification reaction produces monomers most probably in the form of Zn-hydroxo species. Once the monomer concentration reaches supersaturation, ZnO clusters form.

The microwave assisted benzyl alcohol route has also been employed for the preparation of ZnO doped with variety of metals, such as Co, Ni, Fe, Mn, and V [151]. ZnO-based magnetic semiconductor nanocrystals with high concentrations of dopants were synthesized by this method. For example, homogeneous distributions of Co in $Co_xZn_{1-x}O$ were achieved up to $x = 0.2$. Higher loadings of cobalt resulted in separation of a Co_3O_4 phase. Room temperature ferromagnetic behavior was observed in the case of Fe doped ZnO. Other interesting work from the Niederberger group describes benzyl alcohol based microwave assisted synthesis of monodispersed Sb-doped SnO_2 nanocrystals and their application as transparent electrodes in thin film optoelectronic devices [152].

Microwave assisted synthesis in benzyl alcohol was also found to be an efficient method for the preparation of metallophosphates. Bilecka et al. [153,154] obtained highly crystalline, well defined $LiFePO_4$ and $LiMnPO_4$ mesocrystals with sizes of 50 and 200 nm, respectively. The precursor solution

for $LiFePO_4$ was prepared by the addition of H_3PO_4 to a mixture of lithium chloride and iron(II) acetate in benzyl alcohol. For $LiMnPO_4$ synthesis, H_3PO_4 was combined with a solution of manganese(II) acetylacetonate and lithium ethoxide. The reactions were carried out at 180 °C for 3 min with the microwave reactor frequency operating at 2.45 GHz. This work was followed by a study focused on the doping $LiFePO_4$ with Mn, Ni, Zn, Al, and Ti [154]. The incorporation of different dopants in the $LiFePO_4$ lattice in various concentrations allowed modification of the specific charge capacities and achieved the desired characteristics for application in Li-ion batteries. In comparison to undoped $LiFePO_4$ prepared by the same synthetic approach, the doped powders showed significantly better electrochemical performance.

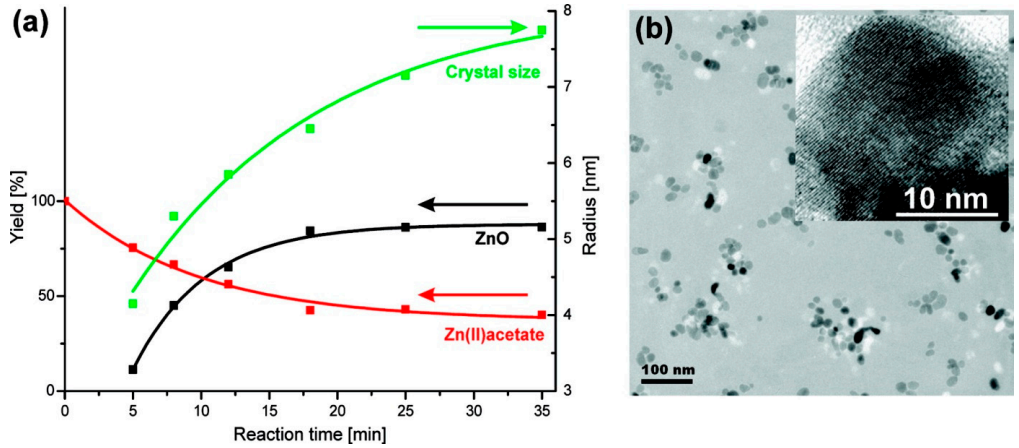

Figure 3. (**a**) Time-dependent evolution of the crystal size (green curve), yield of ZnO powder (black curve), and zinc acetate concentration (red curve) at 120 °C; (**b**) TEM overview image of ZnO nanoparticles obtained at 120 °C after 3 min (inset: high resolution transmission electron microscopy (HRTEM) image of one particle). Reproduced with permission from [40]. Copyright American Chemical Society, 2009.

The polyol microwave assisted synthesis of TiO_2 under non-hydrolytic conditions was developed in the group of Morselli and is included in this review because of its similarity to benzyl alcohol route (polyethylene glycol is used as a high-boiling solvent, surfactant, and oxygen source) [155]. This innovative approach utilizes $TiCl_4$ as a precursor. The reactions were performed in sealed tubes and heated at 170 °C for 25 min under microwave irradiation. According to XRD analysis, all samples are composed of pure anatase NPs and are well dispersed due to the residual PEG chains bonded to the nanoparticle surface, which prevent them from aggregating. The particle size distributions obtained from the transmission electron microscopy (TEM) data ranges from 4 to 8 nm. Oleylalcohol works similar to benzyl alcohol and polyethylene glycol and has also been used for the preparation of metal oxide nanoparticles [156].

2.9. Ether Elimination

The formation of oxo bridges in niobium alkoxides upon heating was first observed by Bradley et al. [55,157]. This reaction principle was later utilized for the synthesis of other oxide-alkoxide molecular species (Ti, Ba-Mo, Na-W, Na-Mo, etc.) [158–160], polyoxovanadate and molybdate clusters [161] and finally for the preparation of metal oxide nanoparticles [56,162,163]. The synthesis was often performed in alcoholic solutions as the protic solvent facilitates the condensation [56]. A part of this research area therefore coincides with the benzyl alcohol route of metal oxide nanoparticles synthesis [56]. However, more recently, carbonyl compounds such as acetone, acetaldehyde or acetophenone were shown to participate in the reaction and promote the formation of metal oxides [164]. Acetals are formed as organic products of the condensation (Scheme 8). Both conventional

and microwave heating of metal alkoxides in acetophenone were shown to provide highly crystalline nanoparticles of $BaTiO_3$, and MFe_2O_4 (M = Mn, Fe, Co, Ni), and this method therefore represents an alternative to the benzyl alcohol route [56,165].

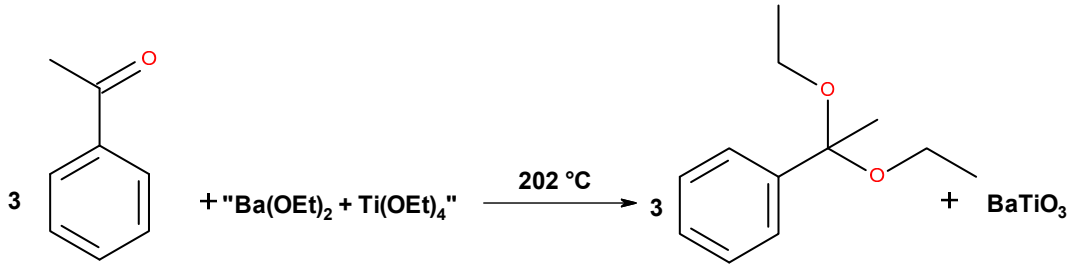

Scheme 8. Reaction of barium and titanium ethoxides with acetophenone producing acetal and $BaTiO_3$. Reproduced with permission from [56]. Copyright John Wiley and Sons, Inc., 2009.

2.10. Twin Polymerization

Another novel non-aqueous route for the synthesis of high-surface-area metal oxide nanoparticles involves so-called twin polymerization (TP) [166]. This technique was developed by Spange et al. as a method for the preparation of high-surface-area metal oxides and nanoparticles [167], such as SiO_2 [168,169] and TiO_2 [170]. The concept underlying this synthetic route is based on the reaction of a well-defined metal-containing monomer leading to interpenetrating composite networks consisting, for example, of a metal oxide and a polymer (Scheme 9). Recently, this approach was extended to a process of simultaneous twin polymerization (STP), in which two well-defined precursors are polymerized simultaneously to produce a single organic homopolymer and nanoscaled mixed metal oxide phases. Leonhardt et al. applied the simultaneous twin polymerization method in the synthesis of mesoporous (165–378 $m^2 \cdot g^{-1}$) SnO_2-SiO_2 hybrid materials [166]. The reaction mixture consisted of monomers 2,2′-*spirobi*[4*H*-1,3,2-benzodioxasiline] and 2,2′-*spirobi*[4*H*-1,3,2-benzodioxastannine] or their derivatives in a 2:1 molar ratio. The reaction performed at 80 or 100 °C led to organic/inorganic hybrid materials corresponding to phenolic resin, SiO_2 and SnO_2 (Scheme 9). Noteworthy, the addition of an initiator is not required because the reaction is self-initiated as a result of the Lewis acidity of the tin precursors. The products are transformed to SnO_2-SiO_2 mixed oxides by subsequent heat treatment in air (700 °C). Surface areas of the calcined materials ranged from 165 to 368 $m^2 \cdot g^{-1}$ [166].

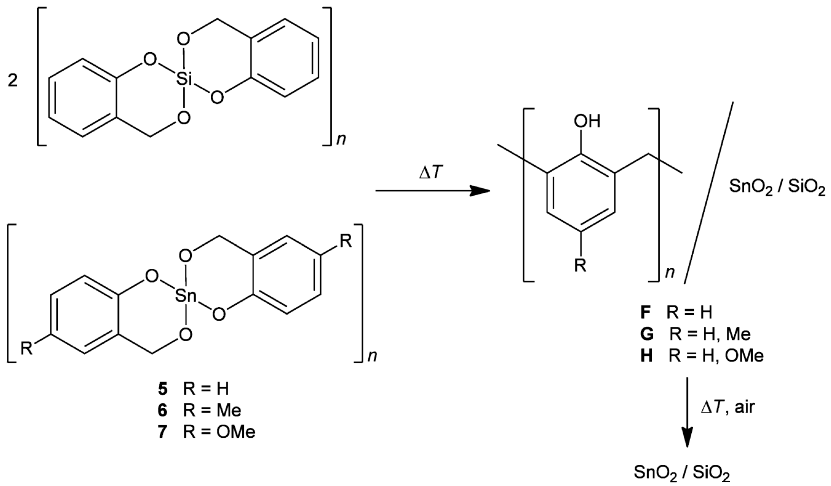

Scheme 9. Simultaneous twin polymerization of 2,2′-*spirobi*[4*H*-1,3,2-benzodioxasiline] and compounds **5**–**7** to give a hybrid material consisting of phenolic resins (e.g., *o*/*o*′ substitution), SnO_2, and SiO_2. Reproduced with permission from [166]. Copyright John Wiley and Sons, Inc., 2013.

3. New Materials

3.1. Surface Area and Pore Size Control

The surface area, pore volume, and pore size distribution are very important parameters of heterogeneous catalysts. The HSG syntheses of silica and other oxides lead mostly to microporous materials through pore collapse because of the high capillary forces exerted during gel drying. This disadvantage can be overcome by supercritical drying affording aerogels, or by the application of templates. Another possibility is to switch to non-aqueous solutions—the organic solvents are easily removed without pore collapse affording materials with both high surface areas and pore volumes in an easy one-step synthesis. This fact presents one of the decisive advantages of NHSG method.

Templating has been used in NHSG chemistry to improve porosity properties and therefore becomes an interesting synthetic approach. It has to be noted that templating techniques under NHSG conditions rely on completely different physico-chemical principles than in water solutions and these principles are only beginning to be understood. The behavior of non-aqueous "oil-in-oil" emulsions was reviewed recently [171].

3.1.1. Without Templates

One of the first examples of the porosity tailoring in NHSG was given by Lafond et al. [79]. Surface area and pore volumes/sizes of titanosilicates prepared by alkyl halide elimination from $SiCl_4$, $TiCl_4$ and diisopropylether/$Si(O^iPr)_4$ were governed by the volume of liquid phase and degree of condensation. Therefore, changing the amount of solvent, reaction time, temperature, and the Si/Ti ratio allowed for tuning surface areas from 450 to 1050 $m^2 \cdot g^{-1}$ and average pore sizes from 2.1 to 6.1 nm. It is noteworthy that even in the absence of templates the pore size distributions were relatively narrow with maxima in the mesoporous region. Interestingly these remarkable porosity properties were not adversely affected by the introduction of organic groups ($SiCl_4$ partially substituted with $MeSiCl_3$ or Me_3SiCl in the synthesis) affording mesoporous silica-titania hybrids with surface areas around 1000 $m^2 \cdot g^{-1}$ [70].

More recently, Barnes et al. presented similar method of porosity control of silica prepared by the NHSG condensation of silicate building block ($Si_8O_{12}(OSnMe_3)_8$) with $SiCl_4py_2$ (py = pyridine) as presented in Section 2.3. The surface area and pore sizes were controlled by the molar ratio of the silicate cube and cross-linking agent used in the synthesis. In other words the average connectivity of $SiCl_4py_2$ played the main role in the porosity properties tailoring (analogous to degree of condensation in previous paragraph) [86]. Generally, the pore sizes were gradually enlarged from micropores all the way to macropores with increasing amount of $SiCl_4py_2$. The highest surface areas (700–1000 $m^2 \cdot g^{-1}$) were observed for the mesoporous materials obtained in the range from 1:2.5 to 1:4 silicate cube to $SiCl_4py_2$ molar ratio (2–2.5 average connectivity = chlorine atoms reacted per one molecule of $SiCl_4py_2$). Importantly, a part of the cross-linking agent could be substituted in the synthesis with metal chloride ($TiCl_4$, $ZrCl_4$) providing single-site metal centers embedded in the silicate matrix without any change of the porosity properties. In other words the trends observed for pure silica matrices can be used for the reliable prediction of porosity properties of metallosilicate catalysts prepared by this method [86].

Somewhat more complicated was the situation with the silicophosphate xerogels prepared by the ester elimination method as described in Section 2.4. The surface areas of these materials depended strongly on the degree of condensation and therefore could be controlled by reaction time and temperature [39] similar to the alkyl halide elimination [79]. All materials prepared were however microporous, and no significant influence on the pore size distribution was observed. The situation changed significantly after the introduction of organic groups via stable Si–C bonds. The average pore size was increased gradually from 2.0 to 11.9 nm after introduction of bridging alkylene units (Si–$(CH_2)_x$–Si, x = 1–3, samples **SiCxSiP**) into the structure. Interestingly similar bridging units between P atoms (P–CH_2CH_2–P and P–C_6H_4–P, samples **SiPC2P** and **SiPC6P**) did not influence the pore size distribution (Figure 4). This difference was explained with the help of solid-state NMR

studies of the xerogel structures. While all microporous samples were built up predominantly from SiO_6 units, mesoporosity was typical for the samples with silicon atoms in the tetrahedral coordination. This environment of the silicon atom was introduced together with the organic groups forming $CSiO_3$ moieties, which built the silicophosphate structure [47].

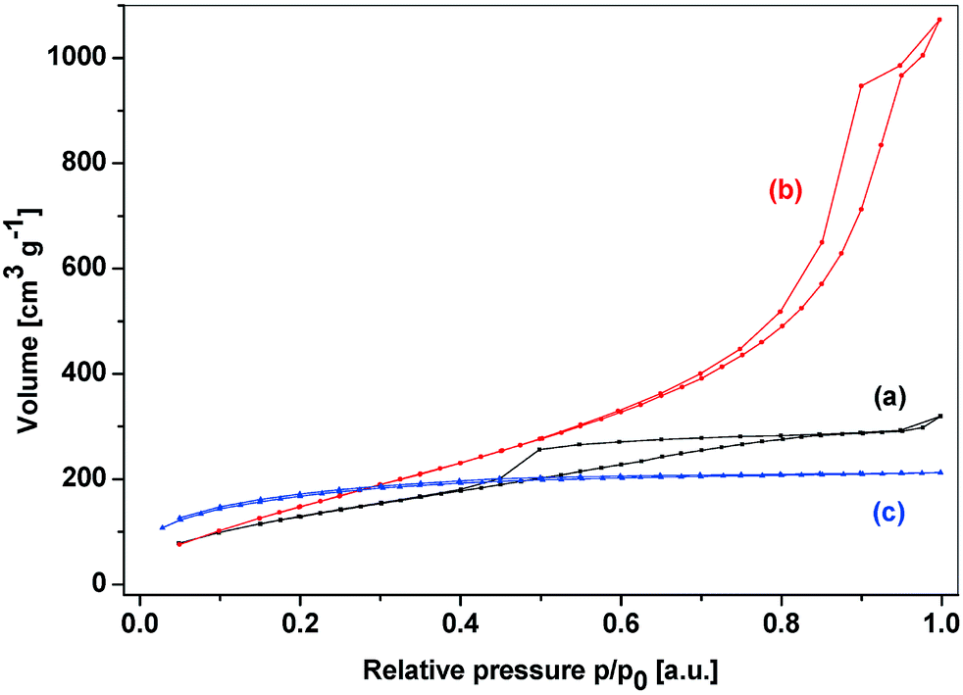

Figure 4. Adsorption-desorption isotherms of xerogels (**a**) **SiC1SiP**; (**b**) **SiC2SiP** and (**c**) **SiPC6P**. Reproduced with permission from [47]. Copyright Royal Society of Chemistry, 2015.

3.1.2. With Templates

The use of structure-directing agents for the generation of well defined ordered porous systems introduces several new possibilities in non-hydrolytic sol-gel chemistry. Interesting work related to these concepts has been reported by the groups of Pinnavaia [172] and Stucky [173]. Stucky´s group developed a simple and general procedure for the preparation of ordered large-pore metal oxides (TiO_2, ZrO_2, Nb_2O_5, SnO_2) and mixed metal oxides ($SiAlO_y$, Al_2TiO_y, $ZrTiO_y$, $SiTiO_y$, ZrW_2O_y) [173]. The use of amphiphilic poly(alkylene oxide) block copolymers as structure-directing agents in non-aqueous protic solutions was crucial for organizing the mesoporous network-forming metal oxide species. The approach presented by Stucky's group uses the conditions that promote a slow hydrolysis (vessel opened to the ambient atmosphere) of the metal chlorides in ethanol and allows for the self-assembly and formation of amorphous inorganic wall structures [173]. The multivalent metal species can associate with the hydrophilic PEO moieties. The ordered inorganic/polymer composite is then formed by cross-linking and polymerization. This approach allows one to produce thermally stable mesoporous metal oxides with robust inorganic frameworks and thick channel walls. For example Si–O–Ti mixed oxides prepared by Yang et al. [173] reveal two-dimensional hexagonal mesostructures with lattice constants of a_0 = 12.2 and 11.0 nm for as-prepared and calcined samples, respectively. Continuous pore/channel walls have thicknesses of 3–5 nm. Adsorption/desorption isotherms of the Si–O–Ti and Si–O–Al calcined mixed oxides exhibit large hysteresis loops referred to as H1-type. Specific surface areas and pore sizes of these materials found by BJH analyses were 310–495 $m^2 \cdot g^{-1}$ and 5–10 nm, respectively.

The next type of synthetic method employing block copolymer templates was developed by the Tilley group [41,174]. In this case, the multicomponent metal oxides were prepared via the thermolytic

decomposition of molecular precursors in nonpolar media in the presence of block copolymers. Within this work, the mixed-element oxides $ZrO_2{\cdot}4SiO_2$, $Ta_2O_5{\cdot}6SiO_2$ [175], $Ga_2O_3{\cdot}6SiO_2$, $Fe_2O_3{\cdot}6SiO_2$, and $AlPO_4$ have been synthesized. The pore radii ranged from 1.0 to 3.9 nm, depending on the polymeric templating agent employed. The use of non-polar solvents and molecular precursors which already contain the M–O–M´ moieties is important for the homogeneity of the final product. A well-studied example describes the transformation of $Zr[OSi(O^tBu)_3]_4$ to $ZrO_2{\cdot}4SiO_2$ with the release of the isobutylene and water as byproducts (Equation (16)). Monolithic gels were obtained by thermal decomposition in toluene at 135 °C with and without copolymer templates.

$$Zr[OSi(O^tBu)_3]_4 \rightarrow ZrO_2{\cdot}4SiO_2 + 12CH_2{=}CMe_2 + 6H_2O \quad (16)$$

Calcination of the template-free xerogel at 500 °C in O_2 led to a mesoporous material with the surface area of about 550 $m^2{\cdot}g^{-1}$. Notably, N_2 adsorption/desorption isotherms of non-templated mixed oxides displayed a prominent hysteresis loop at p/p_0 = 0.6–1.0 indicating a high degree of textural mesoporosity arising from the intraagregate voids caused by circumstantial packing of different-sized particles. Furthermore, the pore size distribution was wide.

N_2 adsorption/desorption isotherms of the templated product, calcined at 500 °C, reveal steep adsorptions to a relative pressure (p/p_0) of ca. 0.6. This type of isotherm was assigned to "framework-confined" mesoporosity, and is characteristic of pores formed from templated framework channels. Compared to the non-templated sample, the pore size distribution is very narrow. Surface areas and pore volumes range from 450–550 $m^2{\cdot}g^{-1}$ and 0.35 to 0.45 $cm^3{\cdot}g^{-1}$, respectively. Low-angle powder X-ray diffraction (XRD) patterns of the calcined materials contain a single broad diffraction maximum centered at *d* spacings of 10.5–11.5 nm. This is characteristic of a lack of long-range crystallographic order and has previously been reported for disordered silicas with a wormhole type of pore channels. "Wormhole like" motifs with no apparent long-range pore order and with relatively uniform channel spacings were observed by HRTEM microscopy. Using the XRD and pore size data, the walls of templated $ZrO_2{\cdot}4SiO_2$ (6.0 to 8.5 nm) are considerably thicker than the silica walls of MCM-41 (1.0–1.5 nm) or the walls of the mesoporous mixed-element oxides reported by Stucky et al. (3.5–5.0 nm) which could provide high (hydro)thermal stability to these materials [41].

Finally the acetamide elimination extended with the addition of templates (Pluronic P123, F127) as structure directing agents, led to highly homogeneous mixed metal oxides with high surface areas and narrow pore size distributions [48–51]. The addition of structure directing agents allows stiff transparent gels to be obtained. The templates are then removed by calcination in air at 500 °C and the final products exhibit mesoporous character with high surface areas. Copolymer templating leads to the generation of wormhole-type pores with diameters ranging from 2.6 to 9.8 nm. The framework-confined mesoporosity was confirmed by the shape of N_2 adsorption/desorption isotherms and by data obtained from small angle X-ray scattering (SAXS) studies which reveal scattering maxima at low angles. The "wormhole like" motifs with relatively uniform channel diameters were observed by TEM microscopy, especially in the case of Ti–O–Si and Zr–O–Si oxides (Figure 5).

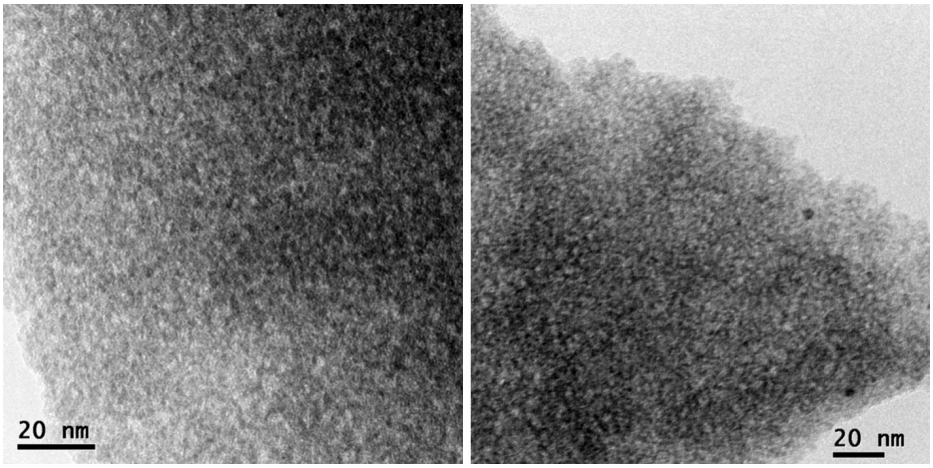

Figure 5. TEM pictures of the zirconosilicate with 43.6 mol % Zr (mol Zr/(mol Si + mol Zr), **SiZrP4-500**) prepared with Pluronic P123 template and calcined at 500 °C. Reproduced with permission from [50]. Copyright Springer, 2015.

The effects of different types of copolymer templates, Si/M, and M/template ratios have also been studied. The influence of different Pluronic templates on textural properties was studied on aluminosilicates and titanosilicates. First, the main differences between Pluronic P123 ($PEO_{20}PPO_{70}PEO_{20}$) and F127 ($PEO_{100}PPO_{65}PEO_{100}$) are that Pluronic F127 has a higher mass and hydrophilicity than P123. We can assume that a bigger template generates bigger pores. This phenomena was observed in the case of aluminosilicates and titanosilicates. In the case of titanosilicates, besides the pore diameter, the surface area and pore volume were also increased by the application of the F127 copolymer [176].

Changing the Si/M ratio also influences the textural properties. The most significant effects were achieved in the case of titanosilicates and zirconium silicates [48,50]. In these cases, the reactions with higher Si/M ratios produce, in addition to the acetamide product, acetic anhydride arising presumably from homocondensation of excess Si–OAc groups (Equation (17)). It is noteworthy, that the condensation producing the anhydride is normally observed at higher temperatures if no Lewis acidic metal centers are present. This condensation is beneficial because it provides new Si–O–Si bonds, which makes xerogels more stable and more porous.

$$\equiv\text{Si–OAc} + \text{AcO–Si}\equiv \rightarrow \equiv\text{Si–O–Si}\equiv + \text{AcOAc} \quad (17)$$

3.2. New Compositions

In recent years, a growing interest has been focused on tuning material properties and specific features toward new application possibilities. This motivation has led to syntheses of new oxidic materials with special compositions. Several examples of new mixed oxides prepared by non-hydrolytic chemistry were published recently. Bouchmella and coworkers reported preparation of mesoporous Re–O–Si–O–Al, Re–O–Al, and Re–O–Si mixed oxides via a one-step non-hydrolytic sol-gel method with the aim of tuning the acidic properties of these solids and thus influence their catalytic performance [177,178]. The authors used the alkyl halide elimination, "ether route", involving the reaction of chloride precursors with diisopropylether at 110 °C. The Re content determined by a nominal Re/(Re + Si + Al) atomic ratio was approximately 0.03. The textural properties in terms of a specific surface area and pore volume depended on the Si/Al ratio, where minima were observed for Si/Al ~0.3. The addition of Re caused a decrease in pore volume. XPS and EDX studies of xerogels showed interesting results on surface and bulk Re/(Re + Si + Al) atomic ratios. While the Re species in as-prepared samples are homogeneously dispersed in the bulk, the calcined xerogels exhibit an increase

of the surface Re/(Re + Si + Al) atomic ratio corresponding to migration of Re to the surface upon thermal treatment (Figure 6). Similar behavior was previously reported for vanadium, molybdenum, and tungsten in Ti–O–V, Ti–O–V–O–Mo, Ti–O–V–O–W, and Si–O–Al–O–Mo mixed oxide catalysts prepared by NHSG and was explained by a low Tammann temperature of the respective metal oxides allowing for their migration at increased temperatures [179–181].

Si–O–Al–O–Mo mixed oxides were prepared via the same non-hydrolytic alkyl halide elimination reaction and with the same goal – tuning the acidity for better catalytic performance [180]. In this study, two reaction parameters were varied systematically: the alumina content (the Si/Al ratio) and the MoO_3 content. A Si/Al ratio of 17 provided materials with high specific surface areas and pore volumes (ca. 500 $m^2 \cdot g^{-1}$ and from 0.9 to 1.6 $cm^3 \cdot g^{-1}$, respectively). MoO_3 content ranging from 5 to 20 wt % was examined and no significant impact on texture was observed. However the catalytic properties relied strongly on the MoO_3 content (Section 4.1).

Oxide materials with the composition V_2O_5-MoO_3-TiO_2 or V_2O_5-WO_3-TiO_2 were prepared from chloride precursors by the same group [181]. Surface areas of the resulting samples ranged from 53 to 109 $m^2 \cdot g^{-1}$ with the pore diameters of about 10 nm. SEM micrographs revealed spherical micrograins of about 2–5 μm formed by an agglomeration of small elementary nanoparticles in the 10–25 nm range. Another family of novel mixed oxides prepared by NHSG is represented by WO_3-SiO_2-Al_2O_3 materials [182]. WO_3 contents were established at 10 and 20 wt %, while the amount of Al_2O_3 ranged from 5 to 20 wt %. These mixed oxides prepared by alkyl halide elimination exhibited surface areas up to 740 $m^2 \cdot g^{-1}$, pore volumes of 1.7 $cm^3 \cdot g^{-1}$, and pore diameters of 9.9 nm. The materials discussed above illustrate that the NHSG approach based on alkyl halide elimination allows for excellent control of composition.

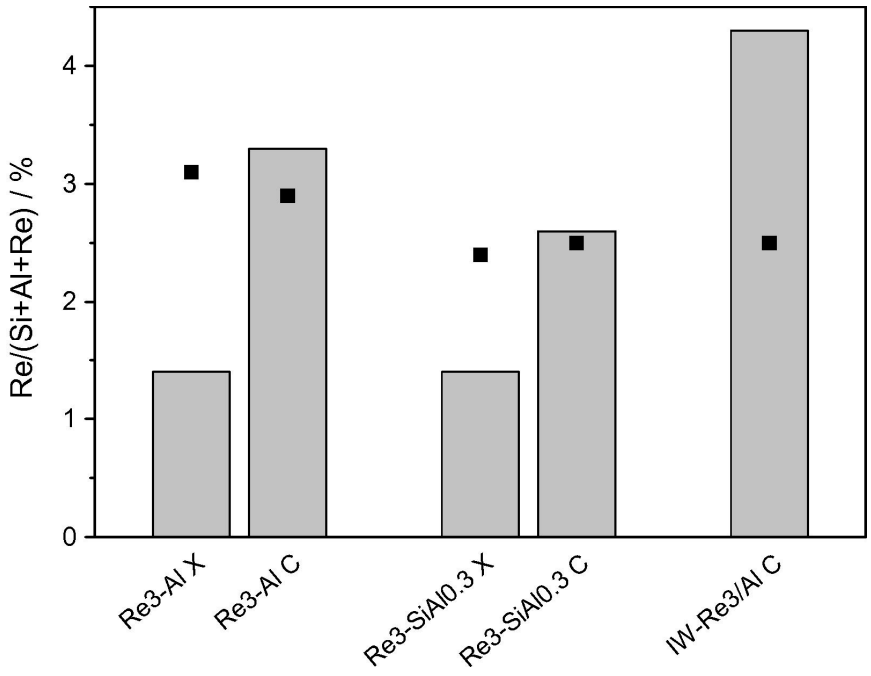

Figure 6. Surface Re/(Si + Al + Re) atomic ratios (XPS, gray bars) and bulk Re/(Si + Al + Re) atomic ratios (EDX, black squares) for xerogels and calcined catalysts. Reproduced with permission from [177]. Copyright Elsevier, 2013.

Caetano et al. [183] described a Co–O–Al–O–Si system prepared by a slightly modified alkyl halide elimination reaction. Firstly, $AlCl_3$ and $CoCl_2$ were reacted with diisopropylether in dichloromethane under reflux. TEOS was added after 1 h of reaction. UV-Vis spectroscopy revealed tetrahedral coordination of Co atoms in the xerogel structure. Co–O–Al–O–Si products calcined at 400 and 750

°C exhibit BET specific surface areas of 53 and 10 $m^2 \cdot g^{-1}$, respectively. Fe–O–Al mixed oxide was prepared in a similar fashion from $FeCl_3$ and $AlCl_3$ in a 1:15 molar ratio [184]. Both materials were acidic and studied as catalysts in hydrocarbon oxidation.

The alkyl halide elimination has, up to now, been presented as a route leading to the preparation of amorphous (mixed) metal oxides and their hybrid derivatives. Nevertheless mixtures of metal chlorides and alkoxides (M = Ti, Zr, Hf, Y, Ce) in strongly coordinating solvents (e.g., oleylamine, trioctylphosphine oxide) at temperatures of 300 °C and higher provide monodisperse nanocrystalline particles of the respective metal oxides [72–77]. Their crystallinity is usually very high and their composition, size, and shape can be controlled. Crystalline HfO_2 nanorods as long as 60 nm and 2.9 nm in diameter were synthesized from $HfCl_4$ and $Hf(OtBu)_4$ if the latter was injected into the reaction mixture in small portions [74].

Recently, templated acetamide elimination was employed for the preparation of Sn–O–Si mixed oxides. According to N_2 adsorption-desorption porosimetry and powder XRD data, the calcined product exhibited mesoporosity with surface area up to 476 $m^2 \cdot g^{-1}$ and contained SnO_2 nanoparticles with a size of ca. 6 nm (Figure 7). Moreover, if as-prepared Sn–O–Si xerogels were heated under N_2 atmosphere, mesoporous nanocomposites consisting of metallic tin, silica and carbon were obtained (Figure 7). These nanocomposite materials can be considered as potential candidates for application in Li-ion batteries.

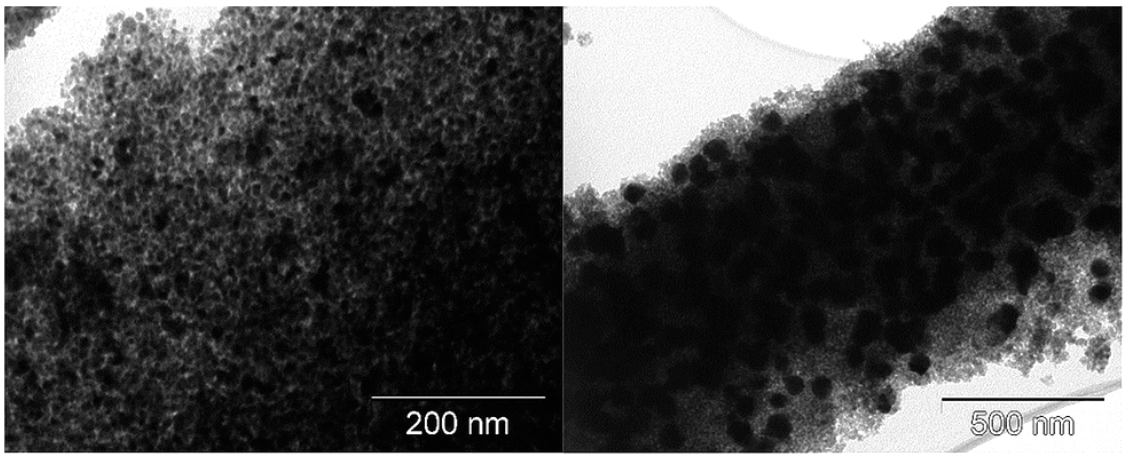

Figure 7. TEM images of SiSnP sample calcined in air (**left**) and heated under N_2 (**right**). Reproduced with permission from [49]. Copyright Royal Society of Chemistry, 2016.

Non-hydrolytic synthesis of Nb–O–V–O–Si mixed oxide catalysts was reported by Moggi [185]. $VO(O^iPr)_3$ and $SiCl_4$ or $Si(OEt)_4$ were added dropwise to stirred suspensions of $NbCl_5$ in hexane. The resulting products were calcined at 550 °C and their BET surface area reached 146 $m^2 \cdot g^{-1}$.

Yttrium-aluminum oxides represent another family of interesting materials which are widely used hosts for lasers and phosphors due to their physical and chemical properties. Non-hydrolytic sol-gel synthesis of YAG was reported by Nassar et al. [132]. The preparation was based on the reaction of $AlCl_3$ and YCl_3 in ethanol in the presence of $EuCl_3$ as a structural probe. The powder XRD analysis of a sintered sample (800 °C) confirmed the presence of $Y_3Al_5O_{12}$ phase. The approach mentioned above was used also for the preparation of YAG doped with Tm^{3+}, Tb^{3+}, and Eu^{3+} [133]. Appropriate metal chlorides were used for the doping. YAG doping with Tm^{3+}, Tb^{3+}, and Eu^{3+} was found to be beneficial for tuning of photoluminescent properties by means of different color emission. The same group utilized a similar synthetic procedure to prepare other luminescent materials as well: several phases of Gd–O–Al mixed oxides doped with Eu^{3+} [186], Eu^{3+}:YVO_4 [134], and Eu^{3+}:$GdCaAl_3O_7$ [135].

Recently, the Tilley group reported a non-hydrolytic synthesis of high surface area gallium-containing silica materials via the thermal decomposition of a $Ga[OSi(O^tBu)_3]_3 \cdot THF$ molecular

precursor [174]. Thermal decomposition in the presence of Pluronic P123 as a templating agent led to a material containing uniform vermicular pores while non-templated samples gave broad pore size distributions. In the case the thermolysis of $Ga[OSi(O^tBu)_3]_3 \cdot THF$ was performed in the presence of $HOSi(O^tBu)_3$ and Pluronic P123, the resulting Ga:Si ratios could be set from 1:3 to 1:50. However, with increasing silicon content the calcined (500 °C) materials exhibited decreasing surface areas and broader pore size distributions. The highest surface area (636 $m^2 \cdot g^{-1}$) was achieved in the case of templated sample with Ga:Si = 1:3. It should be noted, that resulting products exhibited both Lewis and Brønsted acidity. The density of acid sites changed with the silicon content with Brønsted sites increasing at higher silicon loadings while Lewis acidity decreased.

Bismuth vanadate represents another interesting material with a novel composition prepared via the non-hydrolytic microwave-assisted approach based on the concept of twin polymerization [187]. Reactions were performed with the use of bismuth(III) ^{t}butoxide and vanadium(V) oxytri(^{t}butoxide) precursors. These precursors were dissolved in toluene followed by addition of stoichiometric amounts of a polymerizable alcohol (2-methoxybenzyl alcohol; 2,4-dimethoxybenzyl alcohol) or a non-polymerizable alcohol (2-(2-thienyl)isopropyl alcohol). Afterwards trifluoromethanesulfonic acid was added into the reaction mixture and microwave treatment (140 °C, 30 min) was applied. The resulting monoclinic $BiVO_4$ nanoparticles exhibited sizes ranging from 42 to 78 nm and were used as photocatalysts.

Another research group developing new materials by NHSG approach is led by Lind. One of their research topics is the synthesis of crystalline ternary and quaternary metal oxides with $A_2M_3O_{12}$ stoichiometry (A = Al, Sc, Fe, In, Ga, Y, Mg-Zr, Mg-Hf, etc.; M = Mo or W) that exhibit negative thermal expansion (NTE) [62–65,188,189]. The intrinsic advantage of NHSG chemistry—a high homogeneity of element mixing was fully exploited for NTE materials preparation. The synthetic protocols followed the alkyl halide elimination, ether route, with some minor modifications. For example acetonitrile was shown to provide better results than dichloromethane in terms of products homogeneity and crystallization behavior. In most cases significantly lower temperatures (400–700 °C vs. 1000–1500 °C) were needed to obtain desired crystalline materials from the dried amorphous products of the NHSG reactions in comparison to conventional methods (e.g., high temperature ball milling). Scandium, indium, and iron molybdates were obtained in the crystalline form at temperatures as low as 230 °C [62]. Moreover a new polymorph of $Y_2Mo_3O_{12}$ thermodynamically stable below 550 °C was observed (*Pba2*, Figure 8) [64] and a completely new compound $Ga_2Mo_3O_{12}$ was prepared from $GaCl_3$ and $MoCl_5$. This thermodynamically unstable ternary oxide was obtained through the homogeneous mixing of Ga and Mo at the atomic level. The resulting solid decomposes to a mixture of Ga_2O_3 and MoO_3 at 650 °C [65].

Metal sulfides present another interesting group of compounds which are relatively new to NHSG. Their synthesis was accomplished by the Lind group via changing again the protocol of the alkyl halide elimination, ether route. The diisopropylether, which works as an oxygen donor in the original synthesis of metal oxides, was substituted with either di^{t}butyl sulfide or hexamethyldisilathiane as the sulphur sources. A variety of metal sulfides were prepared by this method (Fe, Cu, Ta, Mo, etc.) [190–192]. Its main advantage is that it provides pure oxygen free metal sulfides. There is no need to calcine the products in H_2S owing to intrinsic water and oxygen free conditions of the NHSG syntheses. Another non-aqueous approach providing metal sulfides was presented recently. In this case, the benzyl alcohol route was modified in such a way that benzylthiol was used as the solvent, capping agent, and sulphur source. Nanocrystalline tin and zinc sulfides were prepared [193].

The synthesis of metal fluoride materials has also seen application in non-aqueous chemistry [194]. One synthetic strategy involves the thermolytic decomposition of metal fluoroacetates. Another route strongly resembles HSG approach, however HF in organic solvents is used instead of water in reactions with metal alkoxides and acetates. These syntheses provide molecular compounds (e.g., metal alkoxide fluorides) in the first step and nanoscale metal fluorides after the heat treatment in the second step. Fluorolytic sol-gel chemistry was recently reviewed by Kemnitz et al. [194].

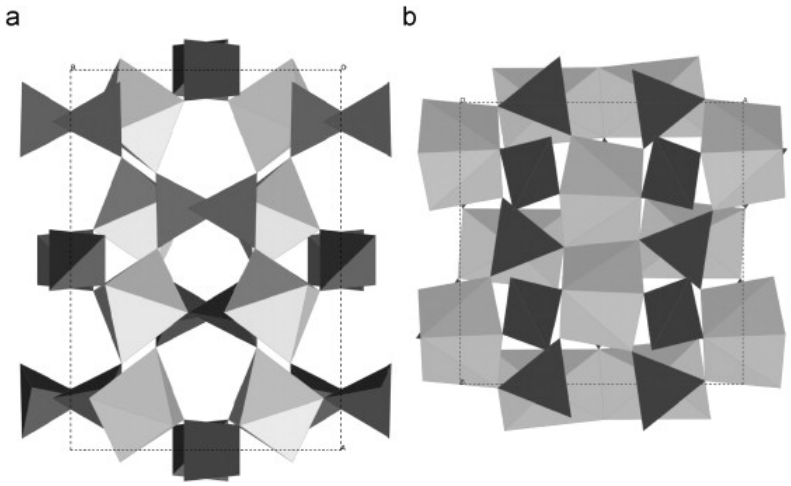

Figure 8. Crystal structures of the (**a**) *Pbcn* and (**b**) *Pba*2 polymorphs of $Y_2Mo_3O_{12}$ viewed down the *z*-axis. Dark tetrahedra are MoO_4 units, and light polyhedra represent 6- and 7-coordinate yttrium, respectively. Polyhedra are only connected via corner-sharing in the *Pbcn* structure, while edge-shared YO_7-units are present in the *Pba*2 polymorph. Reproduced with permission from [64]. Copyright Elsevier, 2007.

Finally, metal phosphates have been prepared by NHSG methods as well since they offer advantages over HSG syntheses. The use of aqueous phosphoric acid leads to rapid precipitation in many cases, while phosphoric acid esters are stable towards water and therefore not suitable for the syntheses relying on hydrolysis. Moreover the P–OH groups do not condense in aqueous solutions to form P–O–P bridges unlike the Si–OH groups [195]. For these reasons the NHSG approach has become an important synthetic method providing metal phosphates. We have already presented the synthesis of silicophosphates and their hybrid derivatives by Styskalik et al. [39,47] via ester elimination and lithium iron phosphate and related compounds by Bilecka et al. [153,154] via the benzyl alcohol route. This reaction pathway was also used to prepare nanocrystalline Ti, Zr, V, Y, Ce, and La phosphates [196]. Several other examples should also be mentioned in this context. Silicophosphates were prepared from anhydrous phosphoric acid and tetraalkoxysilanes by Jähningen et al. [197,198] and Tokuda et al. [199]. Hybrid silicophosphates with various organic groups were prepared by solventless condensations of anhydrous phosphoric acid with alkyl- and arylchlorosilanes by the Takahashi group [200–203]. The preparation of aluminophosphates and molecular building blocks based on Al–O–P bonds by non-aqueous condensations was reported by Pinkas et al. [204,205]. The alkyl halide route has been used to prepare NASICON [206] and metal phosphates and phosphonates of Si, Ti, and Zr [207].

4. New Applications

Materials prepared by NHSG chemistry have found useful application in many fields. For example, exceptionally porous alumina foams have been produced by heat treatment of $AlCl_3{\cdot}O^iPr_2$ in CH_2Cl_2 on an industrial scale since 2001 and used as insulating materials, as already reviewed [15,208,209]. Four main areas of recent interest are identified in the context of this review: heterogeneous catalysts, luminescent materials, catalyst supports, and Li-ion battery electrodes. These four areas will be briefly discussed and some leading examples given in the following section. Recent works related to non-hydrolytic syntheses of mixed oxides and their applications are listed in Table 1.

Table 1. Examples of application of materials prepared by non-hydrolytic sol-gel (NHSG).

Mixed Oxide	Non-Hydrolytic Synthetic Route	Application	References
Al-Si	acetamide elimination	aminolysis catalyst	[51]
Zr-Si	acetamide elimination, alkyl halide elimination	aminolysis, MPV, Friedel-Crafts catalysts	[50,210]
Sn-Si	acetamide elimination, twin polymerization	aminolysis catalyst	[49,166]
Ti-Si	acetamide elimination, alkyl halide elimination	mild oxidation, epoxidation catalysts	[38,48,211–213]
Fe-Al	alkyl halide elimination (ether route)	mild oxidation catalyst	[184]
Co-Al-Si	alkyl halide elimination (ether route)	mild oxidation catalysts	[183]
Re-Al-Si	alkyl halide elimination (ether route)	olefin metathesis catalyst	[177,178]
Mo-Al-Si	alkyl halide elimination (ether route)	olefin metathesis catalyst	[180,214,215]
Mo-Ti-V	alkyl halide elimination (ether route)	total oxidation catalysts	[179,181]
W-Ti-V	alkyl halide elimination (ether route)	total oxidation catalysts	[179,181]
Nb-V-Si	alkyl halide elimination	oxidative dehydrogenation catalyst	[185]
Ga-Si	thermal decompositon of $Ga[OSi(O^tBu)_3]_3 \cdot THF$	Lewis acid catalyst	[174]
Si-P	ester elimination	Brønsted acid catalyst	[95]
$BiVO_4$	microwave assisted twin polymerization	photocatalyst	[187]
TiO_2	ether elimination (chitosan templated)	photocatalyst	[142]
TiO_2	alkyl halide elimination (alkoxide route)	photocatalyst, S, N doped	[216]
Y-V	alkyl halide elimination	luminescent materials, Ln^{3+} doped	[134]
Y-Al	alkyl halide elimination	luminescent materials, Ln^{3+} doped	[132,133,137,139]
Gd-Ca-Al	alkyl halide elimination	luminescent materials, Ln^{3+} doped	[135]
Gd-Al	alkyl halide elimination	luminescent materials, Ln^{3+} doped	[186]
Ln-P	benzyl alcohol route, microwave assisted	luminescent materials, Tb^{3+} doped	[196]
Ti-V	alkyl halide elimination (ether route)	Li-ion batteries	[217]
$Li_4Ti_5O_{12}$	benzyl alcohol route	Li-ion batteries	[218]
$LiFePO_4$	benzyl alcohol route, microwave assisted	Li-ion batteries	[153,154]
$LiMnPO_4$	benzyl alcohol route, microwave assisted	Li-ion batteries	[153]
SnO_2/GO	benzyl alcohol route, microwave assisted	Li-ion batteries	[219]
Fe_3O_4/GO	benzyl alcohol route, microwave assisted	Li-ion batteries	[220]
ZnO	benzyl alcohol route, microwave assisted	magnetic semiconductors, doped	[151]
SnO_2	benzyl alcohol route, microwave assisted	optoelectonic devices, Sb doped	[152]
Si-P	ester elimination	catalyst support	[94]
SiO_2	alkyl halide elimination (alkoxide route)	catalyst support	[221–223]

4.1. Heterogeneous Catalysts

The specific properties and features of mixed oxides open a large area of the application possibilities in heterogeneous catalysis. Innovative ideas of catalysts applications and their design require specific catalytic sites with a high activity, stability, and recyclability. The non-hydrolytic sol-gel chemistry offers a promising pathway for the targeted preparation of heterogeneous catalysts with control of structure, texture, and composition.

There are many papers devoted to SiO_2-TiO_2 epoxidation and mild oxidation catalysts. The crucial condition for catalytic efficiency is the presence of atomically dispersed tetrahedral Ti(IV) atoms. These sites introduce Lewis acidic centers required in catalytic reactions, and arise when Ti atoms substitute Si in silicon dioxide. Therefore, the homogeneity of atomic mixing is of crucial importance for the catalytic activity. Cojocariu et al. reported that the oxidation of various aromatic and sulphur compounds, such as anthracene, styrene, cyclooctene, and phenylsulfide with aqueous solutions of H_2O_2 or TBHP (^{t}butylhydroperoxide) is promoted by titanosilicate catalysts prepared via alkyl halide elimination [212,213]. It was found that the catalysts exhibit high catalytic activities, much higher than those reported for the conventional TS-1 catalyst. The mesoporous nature of the NHSG catalysts was apparently their main advantage over microporous TS-1 when working with bulky substrates. The epoxidation reaction of cyclohexene with cumyl hydroperoxide (CHP) catalyzed by SiO_2-TiO_2 xerogels was described by Lafond et al. [211]. In this particular reaction, a NHSG-prepared titanosilicate catalyst achieved conversions higher than 90%. Mesoporous titanosilicate catalysts prepared by templated acetamide elimination reaction were recently reported [48]. Catalysts were tested for the epoxidation of cyclohexene similar to the work of Lafond et al. Conversions of 96% were achieved with high selectivity for the epoxide. A comparison of the properties and activities of some NHSG [48] and conventional SiO_2-TiO_2 catalysts shows that NHSG samples give comparable or better results (Table 2).

Table 2. Reaction parameters and comparison of results of the cyclohexene epoxidation with different TiO_2-SiO_2 catalysts. Reproduced with permission from [48]. Copyright Springer, 2015.

Catalyst	Ti [wt %]	Ti in Catalyst [mmol]	Cyclohexene [mmol]	CHP [mmol]	T [°C]	SA_{BET} [$m^2 \cdot g^{-1}$]	Epoxide Yield [%]	TON [a]
SiTi1 [48]	12.48	0.13	25	5	65	12	69	26
9SiTi [48]	3.72	0.03	25	5	65	-	77	126
SiTiP2-500 [48]	27.43	0.28	25	5	65	325	65	12
SiTiP2-500N [48]	22.01	0.23	25	5	65	453	80	16
9SiTiP-500 [48]	8.09	0.09	25	5	65	442	96	52
9SiTiP-500N [48]	6.64	0.03	25	5	65	615	96	158
SiO_2.TiO_2 (NHSG) [211]	7	0.0731	25	5	65	780	91	62
Shell [211]	9	0.0094	25	5	65	200	68	360
SiO_2.TiO_2 xerogel [224]	15	0.157	25	5	65	552	38	12
SiO_2.TiO_2 aerogel [224]	15	0.157	25	5	65	677	49	16
10LT HSG aerogel [225]	6	0.125	77	13.4	60	683	87	93
20LT HSG aerogel [225]	12	0.251	77	13.4	60	674	93	50

[a] TON = (mol epoxide) × (mol Ti)$^{-1}$, after 2 h.

SiO_2-ZrO_2 oxides prepared by NHSG reactions were reported as catalysts for Friedel-Crafts alkylation [210], MPV reduction [50], and aminolysis reactions [50]. Kaper et al. reported a high surface area (up to 570 $m^2 \cdot g^{-1}$) zirconium silicate catalyst prepared by alkyl halide elimination [210]. The resulting material exhibited high catalytic activity for Friedel-Crafts alkylation reactions between anisole and various alcohols. The best conversions were observed for benzyl alcohol (84%) and 1-phenylethanol (95%) substrates. Mesoporous zirconium silicates (up to 537 $m^2 \cdot g^{-1}$) prepared via templated acetamide elimination were tested as catalysts for aminolysis of styrene oxide and for Meerwein–Ponndorf–Verley (MPV) reduction of 4-^{t}butylcyclohexanone [50]. Lewis acidic sites were studied by pyridine adsorption, and tetrahedrally coordinated Zr atoms were identified by DRUV spectroscopy. The conversions of styrene oxide and 4-^{t}butylcyclohexanone reached up to 96% and 54%, respectively.

Aluminosilicates represent a group of materials with both Lewis and Brønsted acidity. They can be used as catalysts or as supports for other active species. The crucial condition for catalytic activity is the presence of tetracoordinated and pentacoordinated Al atoms. These species can be studied by the ^{27}Al MAS NMR spectroscopy. Recently, mesoporous aluminosilicate catalysts (up to 627 $m^2 \cdot g^{-1}$) prepared via templated acetamide elimination were reported [51]. The products were used in aminolysis reactions, where high catalytic activities were observed. The catalytic activity of SnO_2-SiO_2 mesoporous xerogels in aminolysis of styrene oxide has also been investigated. In this case the conversion of styrene oxide was reasonably high and reached 50% after 1 h [49].

The total oxidation of volatile organic compounds (VOCs) which are released in some industrial processes is currently a frequently discussed topic. Decomposition of these pollutants, represented mostly by chlorinated aromatics, can be catalyzed by so-called total oxidation catalysts. These were prepared by the group of Debecker and were based on MoO_3- and WO_3-V_2O_5-TiO_2 oxides [179,181]. The authors reported high conversions of benzene and chlorobenzene especially in the case of samples with 10 wt % V_2O_5 loadings. The incorporation of Mo and W into catalysts showed promoting effects and increased their efficiency. For example the total oxidation of chlorobenzene reached 93% conversion after 150 min at 300 °C. NHSG derived VOC total oxidation catalysts reported by Debecker et al. [179,181] exhibit a comparable activity to the catalysts prepared by impregnation method on TiO_2 supports [226]. Another class of materials studied by the same group were catalysts for olefin metathesis. They prepared mesoporous mixed oxide based catalysts with the compositions of Mo–O–Si–O–Al [180,214,215] and Re–O–Si–O–Al [177,178]. All samples catalyzed the conversion of propene to ethene and butene with more than 99 % selectivity. In the case of Mo–O–Si–O–Al samples, the best catalysts contained only 5 wt % Al_2O_3 and their activity increased with higher MoO_3 loading. The Re–O–Si–O–Al catalysts exhibited a comparable catalytic activity to the Mo–O–Si–O–Al catalysts. The best catalytic performance was achieved with a sample Re3–SiAl0.3 (ca. 10 wt % Re_2O_7) which produced propene at a specific activity of 45 mmol$\cdot g^{-1} \cdot h^{-1}$. It is important to use a Si–O–Al mixed

oxide as a support because Al atoms significantly increase the acidity of the catalysts according to NH_3-TPD.

There are several reports dealing with non-hydrolytic synthesis of photocatalysts. Hamden et al. described chitosan (CS) templated in situ generation of TiO_2 nanoparticles from $Ti(O^tBu)_4$ [142]. A low crystallization temperature (ca. 150 °C) of anatase was observed. The authors used CS-TiO_2 samples for photocatalytic degradation of aniline in water and under halogen lamp irradiation. The degradation of aniline after 9 h irradiation reached 5% and 33% in the presence of dried (50 °C) and heated (300 °C) CS-TiO_2 photocatalysts, respectively. The work of Albrbar describes visible-light active mesoporous, nanocrystalline N,S-doped and co-doped titania photocatalysts [216]. These samples were synthesized from $TiCl_4$ and $Ti(O^iPr)_4$ in cyclohexane or dimethyl sulfoxide, the latter being used as a S-doping agent. The best photocatalytic activity was achieved by sulphur-doped material with the smallest crystallites and the highest BET surface area. An important feature of these materials is their high adsorption capacity. Finally, the photocatalytic properties of bismuth vanadate ($BiVO_4$) prepared by a non-hydrolytic microwave assisted reaction were described by Hofmann et al. [187]. $BiVO_4$ showed a very high degradation efficiency (>99%) of rhodamine B after 150 min under visible light irradiation. It was shown that the highest efficiency was reached in the case of the smallest $BiVO_4$ crystallites.

4.2. Luminiscent Materials

There are several reports describing the preparation of luminescent materials by non-hydrolytic sol-gel reactions. It has been argued, that luminescent properties strongly depend on the synthetic procedure, composition, homogeneity, and annealing temperature. One of the first examples of NHSG methods used in the synthesis of silica-based phosphor materials was published already in 1997 by Green et al. [227].

More recently, photoluminescent properties of yttrium vanadate with Eu^{3+} as a dopant were investigated by Matos et al. [134]. The europium ion dopant (Eu^{3+}) was added at a mole ratio of 1% relative to the Y^{3+} ion. The YVO_4 phase (crystallite size ca. 43 nm) was formed after heat treatment of the as-synthesized powder at 600 °C. The authors reported interesting luminescent properties depending on the calcination temperature (Figure 9). Excitation spectra of the samples were recorded with the fixed emission wavelength at the Eu^{3+}: $^5D_0$-$^7F_2$ transition. It was found that the excitation of the samples is attributed to the O–V charge transfer (CT) represented by an intense broad band ranging from 250 to 350 nm. The CT band includes transfer from VO_4^{3-} to the $^5L_6$ level as well as the transfer from O to Eu, accounting for the longer lifetime and higher quantum efficiency. The longest lifetime of 0.99 ms and the highest quantum efficiency of 75% were presented in the case of a sample calcined at 800 °C. Higher annealing temperatures resulted in a red shift of the CT band (V–O).

The work of Nassar et al. describes the luminescent properties of NHSG derived Eu^{3+} doped yttrium-aluminum oxide [132,137]. The samples were treated at 800 °C and excited at 394 nm ($^5L_6$ level). The emission spectra displayed $^5D_0 \rightarrow {}^7F_J$ (J = 0, 1, 2, 3 and 4) emission lines of Eu^{3+}. Excitation near the emission level $^5D_0$ decreased the lifetime as observed in case of $^5L_6 \rightarrow {}^5D_2$ level (ca. 0.4 ms). Emission of different colors was achieved using the same host (YAG) but different dopants (Tm^{3+} and Tb^{3+}) [133,139].

A $GdCaAl_3O_7$ aluminate matrix was prepared by Matos et al. [135]. Europium ion Eu^{3+} was used as a structural probe in a molar ratio of 1% relatively to Gd^{3+}. The characteristic diffraction of $GdCaAl_3O_7$ at $2\theta = 31°$ appeared when the xerogel was heated to 800 and 1000 °C. The CT band maxima obtained for samples treated at 800 and 1000 °C appeared in the region ca. 270 nm, while samples treated at 600 °C exhibited this band at 280 nm. Excitation at 391 nm ($^5L_6$ level) leads to emission in all the samples. Reported data showed that $GdCaAl_3O_7$ with Eu^{3+} is a candidate for application in the field emission color display technology. The emission maximum was found to be the $^5D_0$-$^7F_2$ band which corresponds to the red emission of the Eu^{3+} ion. Similar results were achieved also for gadolinium-aluminum mixed oxides doped with Eu^{3+} ions [186].

Unlike the syntheses presented above, heat treatment was not necessary in the case of nanocrystalline $La_{0.4}Ce_{0.45}Tb_{0.15}PO_4$ and $Ce_{0.85}Tb_{0.15}PO_4$ prepared by the microwave-assisted benzyl alcohol route. The residual organic groups were effectively depleted, nanoparticles were highly crystalline, and showed good luminescent properties. Their preparation was performed at temperatures as low as 180 °C and that presents an important advantage of this synthetic approach [196].

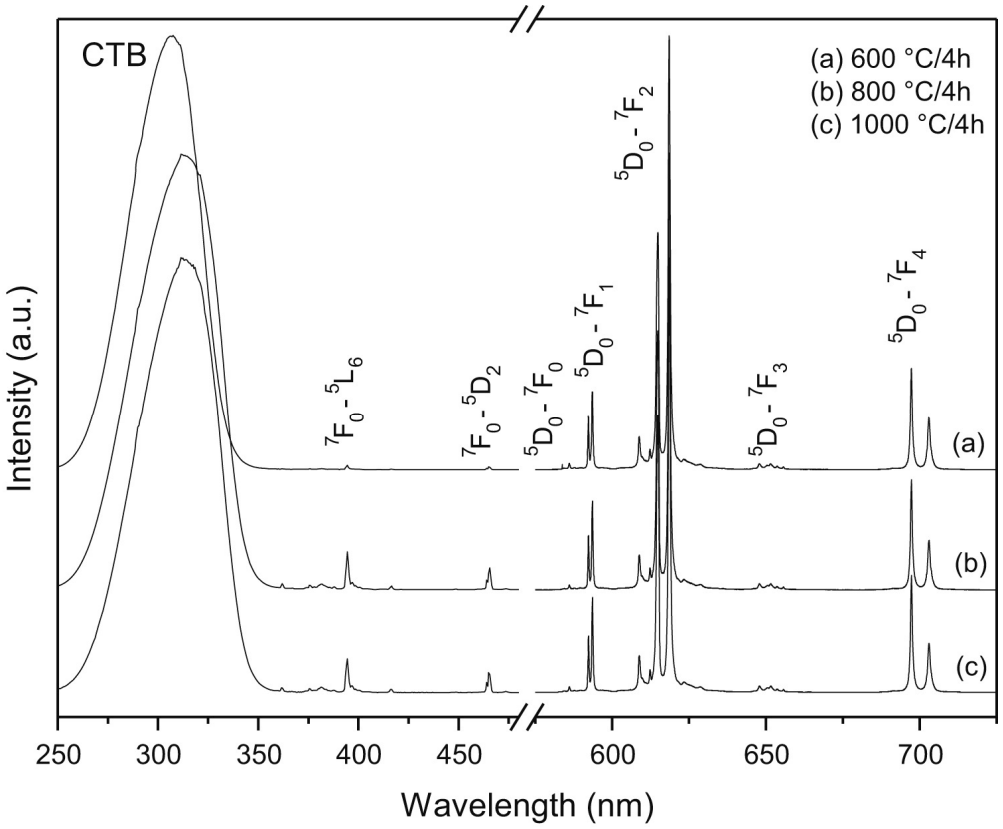

Figure 9. Excitation (λ_{em} = 616 nm) and emission (λ_{exc} = CTB) spectra of the Eu^{3+} ion in the YVO_4 host treated at (**a**) 600; (**b**) 800; and (**c**) 1000 °C for 4 h. Reproduced from [134]. Copyright Elsevier, 2014.

4.3. Electrodes in Li-Ion Batteries

Non-hydrolytic sol-gel syntheses were also employed in the preparation of mixed oxides and phosphates used in batteries. Due to good reaction control and high homogeneity of final products, non-hydrolytic methods offer promising pathways for electrode materials syntheses. The benzyl alcohol route was used for the preparation of $LiFePO_4$, $LiMnPO_4$, and $Li_4Ti_5O_{12}$ materials [153,154,218]. $LiFePO_4$ prepared by Bilecka et al. exhibited excellent electrochemical performance including high discharge capacities of ca. 150 $mAh \cdot g^{-1}$ with a capacity loss of only 5–10% after 160 cycles (Figure 10) [153]. In the case of $LiMnPO_4$ a capacity of ca. 125 $mAh \cdot g^{-1}$ was observed. Reported results indicate that the mesocrystalline particle morphology of synthesized $LiFePO_4$ is optimal for electrochemical performance. More recently, Bilecka et al. reported Mn^{2+}, Ni^{2+}, Zn^{2+}, Al^{3+}, and Ti^{4+} doped $LiFePO_4$ by the microwave assisted benzyl alcohol route [154]. The presented work demonstrated that the doping of $LiFePO_4$ improved electrochemical properties (especially the discharge capacities). For example the material $LiNi_{0.07}Fe_{0.93}PO_4$ exhibited capacity of 163 $mAh \cdot g^{-1}$ after 300 cycles with a loss of only 3%.

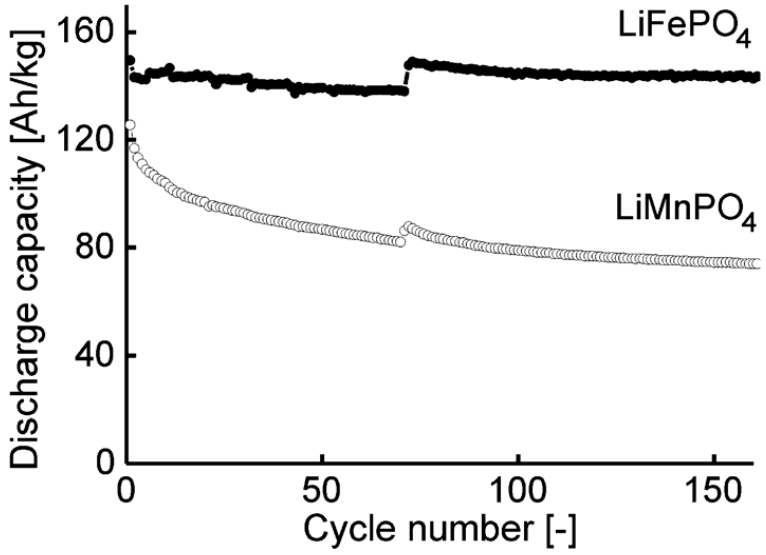

Figure 10. Typical discharge capacity per unit mass (specific charge) of $LiFePO_4$ and $LiMnPO_4$ in composite. Reproduced with permission from [153]. Copyright Royal Society of Chemistry, 2009.

The work of Yu et al. [218] describes nanostructured micrometer-sized hierarchical spinel $Li_4Ti_5O_{12}$ nanostructures prepared via the benzyl alcohol method from metallic lithium and $Ti(O^iPr)_4$ at 250 °C. It was found that annealing at 750 °C improves the electrochemical performance, which reaches the theoretical capacity of $Li_4Ti_5O_{12}$ and displays a loss of less than 5% after 200 cycles. The capacities after 200 cycles at the current density of 1 C (175 $mA \cdot g^{-1}$) were 110 and 148 $mAh \cdot g^{-1}$ for the as-prepared and calcined samples, respectively.

SnO_2/graphene and Fe_3O_4/graphene heterostructures for Li-Ion batteries were also prepared via one pot microwave assisted reaction based on benzyl alcohol route [219,220]. The reaction of tin(IV) chloride and iron(III) acetylacetonate precursors in benzyl alcohol in the presence of graphene oxide (GO) resulted in tin and iron oxide nanoparticles bound to the graphene surface. Benzyl alcohol acts as a reactant for metal oxide synthesis and as a reducing agent for the partial reduction of GO. The authors demonstrated that at a current density of 1600 $mA \cdot g^{-1}$, the capacities for the SnO_2/graphene and Fe_3O_4/graphene composites lie above 300 and 400 $mAh \cdot g^{-1}$, respectively. Moreover, it was found that a higher graphene/metal oxide ratio is beneficial for the higher capacity of the composites.

Recently, the lithium insertion properties of metal oxide microspheres prepared via non-hydrolytic sol-gel were studied by Escamilla-Pérez [217]. It was found that conductivity of TiO_2–V_2O_5 materials was significantly higher compared to TiO_2, but the specific capacity was not increased. The values obtained for TiO_2 and TiO_2–V_2O_5 (5 wt % V) reached 125 and 115 $mAh \cdot g^{-1}$, respectively, at a current density of 336 $mA \cdot g^{-1}$.

4.4. Catalyst Supports

It is noteworthy that NHSG materials possess different groups on the surface than silica prepared by conventional methods (e.g., Si–Cl, Si–OAc, Si–OEt, etc. vs. Si–OH) and therefore their reactivities differ significantly. Silica-based materials containing catalytic centers, such as metallocenes or methylaluminoxanes (MAO), were reported by the group of Dos Santos [221,222]. The preparation of their silica supports is based on the reaction between $SiCl_4$ and $Si(OEt)_4$ in toluene with the addition of a catalytic amount of $FeCl_3$. Metallocene or MAO is then added into the silica precursor mixture. Unfortunately, resulting materials exhibit low surface areas and poor catalytic activities. This behavior may be caused by some side reactions of MAO with silica. Moreover, access to the active centers encapsulated inside an almost non-porous silica support is strongly hindered. An increase in catalytic

activity was achieved by increasing metallocene concentration in these materials [222]. The same group also described alizarin incorporated silica materials with potential application as pH sensors [223].

The surface reactivity of silicophosphates and their hybrid derivatives prepared by ester elimination was recently investigated. It was possible to graft highly acidic P–OH groups and pure tetrahedral Al atoms onto the surface. Potential application of these materials was demonstrated in α-methylstyrene dimerization where they were used as acidic heterogeneous catalysts [94]. Very recently Kejik et al. reported the preparation of microporous and mesoporous organosilicates [110]. These materials, synthesized via a novel non-hydrolytic sol-gel method from $Si(OAc)_4$ and polyphenols, exhibit high surface areas and their porosity can be controlled by the type of linker used.

An interesting area of future investigation is the combination of NHSG method and click chemistry. Click chemistry is already widely used for the surface grafting. However, as far as we know, it has not been used on NHSG supports yet [228]. Click reactions often need anhydrous conditions [229,230]. Moreover the introduction and homogeneous dispersion of organic groups in metal oxides by NHSG were shown to be successful in many cases thus providing ideal conditions for surface grafting by click chemistry.

5. Overview and Conclusions

This review summarizes recent progress in the area of non-hydrolytic sol-gel chemistry. The main NHSG methodologies have been described with emphasis on new synthetic pathways, their mechanisms and how these correlate with the homogeneity of final products. The non-hydrolytic condensation reactions reported here offer wide variability in the choice of precursors and allow for the control of the reaction rates resulting in homogeneous products with specific properties and compositions. This review also describes novel materials prepared via NHSG based on mixed metal oxides, silicates and phosphates and their application in the fields of heterogeneous catalysis, photonics, and electrochemistry. Many examples reported here show that NHSG is beneficial for the preparation of mesoporous catalysts with specific active sites and controlled porosity as well as monodispersed mixed metal oxide nanoparticles with specific shapes and sizes. In addition, NHSG methods offer unique surfactant-free syntheses of nanoparticles with non-hydroxylated surfaces, which again are of growing interest in catalysis, sensing, and photonics. They also open access to stable colloids in non-aqueous solvents and hydrophobic nanofillers, with applications in the field of polymer nanocomposites.

In conclusion, the non-hydrolytic sol–gel process provides an important alternative to the conventional sol-gel process. Research in this area is growing rapidly, but much remains to be done to explore all the possibilities and processes in NHSG chemistry. We believe that, due to the beneficial features of non-hydrolytic sol-gel chemistry, it will find increasing application in the design of innovative materials.

Acknowledgments: This research was financially supported by the Ministry of Education, Youth and Sports of the Czech Republic under the project CEITEC 2020 (LQ1601) and Program NPU I (LO1504). This work was also supported as part of the Center for Direct Catalytic Conversion of Biomass to Biofuels (C3Bio), an Energy Frontier Research Center funded by the U.S. Department of Energy, Office of Science, Office of Basic Energy Sciences under Award Number DESC0000997 and DOE BES grant DE-FG02-01ER15259.

Author Contributions: A.S. and D.S. reviewed the literature and wrote the initial manuscript; C.E.B. and J.P. wrote small parts and made helpful suggestions on the content and style of the review.

Conflicts of Interest: The authors declare no conflict of interest.

References

1. Brinker, C.J.; Scherer, G.W. *Sol-Gel Science: The Physics and Chemistry of Sol-Gel Processing*; Academic Press: Boston, MA, USA, 1990.
2. Livage, J.; Henry, M.; Sanchez, C. Sol-gel chemistry of transition metal oxides. *Prog. Solid State Chem.* **1988**, *18*, 259–341. [CrossRef]
3. Hench, L.L.; West, J.K. The sol-gel process. *Chem. Rev.* **1990**, *90*, 33–72. [CrossRef]

4. Danks, A.E.; Hall, S.R.; Schnepp, Z. The evolution of "sol-gel" chemistry as a technique for materials synthesis. *Mater. Horiz.* **2016**, *3*, 91–112. [CrossRef]
5. Faustini, M.; Grosso, D.; Boissière, C.; Backov, R.; Sanchez, C. "Integrative sol-gel chemistry": A nanofoundry for materials science. *J. Sol-Gel Sci. Technol.* **2014**, *70*, 216–226. [CrossRef]
6. Debecker, D.P.; Mutin, P.H. Non-hydrolytic sol–gel routes to heterogeneous catalysts. *Chem. Soc. Rev.* **2012**, *41*, 3624–3650. [CrossRef] [PubMed]
7. Flaig, S.; Akbarzadeh, J.; Dolcet, P.; Gross, S.; Peterlik, H.; Hüsing, N. Hierarchically Organized Silica-Titania Monoliths Prepared under Purely Aqueous Conditions. *Chem. Eur. J.* **2014**, *20*, 17409–17419. [CrossRef] [PubMed]
8. Yu, M.; Liang, M.; Liu, J.; Li, S.; Xue, B.; Zhao, H. Effect of chelating agent acetylacetone on corrosion protection properties of silane-zirconium sol-gel coatings. *Appl. Surf. Sci.* **2016**, *363*, 229–239. [CrossRef]
9. Hutter, R.; Dutoit, D.C.M.; Mallat, T.; Schneider, M.; Baiker, A. Novel Mesoporous Titania-Silica Aerogels Highly Active for the Selective Epoxidation of Cyclic Olefins. *J. Chem. Soc. Chem. Commun.* **1995**, 163–164. [CrossRef]
10. Gisler, A.; Müller, C.A.; Schneider, M.; Mallat, T.; Baiker, A. Titania-silica epoxidation catalysts modified by mono- and bidentate organic functional groups. *Top. Catal.* **2001**, *15*, 247–255. [CrossRef]
11. Gerrard, W.; Griffey, P.F. A Novel Preparation of Boron Phosphate. *Chem. Ind.* **1959**, *1959*, 55.
12. Lindquist, D.A.; Poindexter, S.M.; Rooke, S.S.; Stockdale, D.R.; Babb, K.; Smoot, A.L.; Young, W.E. Boron Phosphate and Aluminum Phosphate Aerogels. *Proc. Ark. Acad. Sci.* **1994**, *48*, 100–103.
13. Goubeau, J.; Christe, K.O.; Teske, W.; Wilborn, W. Über die Silicophosphorsäure und ihre Derivate. *Z. Anorg. Allg. Chem.* **1963**, *325*, 26–42. [CrossRef]
14. Debecker, D.P.; Hulea, V.; Mutin, P.H. Mesoporous mixed oxide catalysts via non-hydrolytic sol-gel: A review. *Appl. Catal. A Gen.* **2013**, *451*, 192–206. [CrossRef]
15. Mutin, P.H.; Vioux, A. Nonhydrolytic processing of oxide-based materials: Simple routes to control homogeneity, morphology, and nanostructure. *Chem. Mater.* **2009**, *21*, 582–596. [CrossRef]
16. Niederberger, M.; Garnweitner, G. Organic reaction pathways in the nonaqueous synthesis of metal oxide nanoparticles. *Chem. Eur. J.* **2006**, *12*, 7282–7302. [CrossRef] [PubMed]
17. Niederberger, M.; Garnweitner, G.; Buha, J.; Polleux, J.; Ba, J.; Pinna, N. Nonaqueous synthesis of metal oxide nanoparticles: Review and indium oxide as case study for the dependence of particle morphology on precursors and solvents. *J. Sol-Gel Sci. Technol.* **2006**, *40*, 259–266. [CrossRef]
18. Djerdj, I.; Arčon, D.; Jagličić, Z.; Niederberger, M. Nonaqueous synthesis of metal oxide nanoparticles: Short review and doped titanium dioxide as case study for the preparation of transition metal-doped oxide nanoparticles. *J. Solid State Chem.* **2008**, *181*, 1571–1581. [CrossRef]
19. Niederberger, M. Nonaqueous Sol-Gel Routes to Metal Oxide Nanoparticles. *Acc. Chem. Res.* **2007**, *40*, 793–800. [CrossRef] [PubMed]
20. Bilecka, I.; Niederberger, M. New developments in the nonaqueous and/or non-hydrolytic sol-gel synthesis of inorganic nanoparticles. *Electrochim. Acta* **2010**, *55*, 7717–7725. [CrossRef]
21. Pinna, N.; Garnweitner, G.; Antonietti, M.; Niederberger, M. A general nonaqueous route to binary metal oxide nanocrystals involving a C–C bond cleavage. *J. Am. Chem. Soc.* **2005**, *127*, 5608–5612. [CrossRef] [PubMed]
22. Garnweitner, G.; Niederberger, M. Nonaqueous and Surfactant-Free Synthesis Routes to Metal Oxide Nanoparticles. *J. Am. Ceram. Soc.* **2006**, *89*, 1801–1808. [CrossRef]
23. Mutin, P.H.; Vioux, A. Recent advances in the synthesis of inorganic materials via non-hydrolytic condensation and related low-temperature routes. *J. Mater. Chem. A* **2013**, *1*, 11504–11512. [CrossRef]
24. Hay, J.N.; Raval, H.M. Synthesis of Organic−Inorganic Hybrids via the Non-hydrolytic Sol-Gel Process. *Chem. Mater.* **2001**, *13*, 3396–3403. [CrossRef]
25. Brook, M.A.; Grande, J.B.; Ganachaud, F. New Synthetic Strategies for Structured Silicones Using $B(C_6F_5)_3$. In *Advances in Polymer Science*; Springer: Berlin, Germany, 2010; Volume 235, pp. 161–183.
26. Thompson, D.B.; Brook, M.A. Rapid Assembly of Complex 3D Siloxane Architectures. *J. Am. Chem. Soc.* **2008**, *130*, 32–33. [CrossRef] [PubMed]
27. Le Roux, C.; Yang, H.; Wenzel, S.; Grigoras, S.; Brook, M.A. Using "Anhydrous" Hydrolysis to Favor Formation of Hexamethylcyclotrisiloxane from Dimethyldichlorosilane. *Organometallics* **1998**, *17*, 556–564. [CrossRef]

28. Wakabayashi, R.; Kawahara, K.; Kuroda, K. Nonhydrolytic Synthesis of Branched Alkoxysiloxane Oligomers $Si[OSiH(OR)_2]_4$ (R = Me, Et). *Angew. Chem. Int. Ed.* **2010**, *49*, 5273–5277. [CrossRef] [PubMed]
29. Hagiwara, Y.; Shimojima, A.; Kuroda, K. Alkoxysilylated-Derivatives of Double-Four-Ring Silicate as Novel Building Blocks of Silica-Based Materials. *Chem. Mater.* **2008**, *20*, 1147–1153. [CrossRef]
30. Bassindale, A.R.; MacKinnon, I.A.; Maesano, M.G.; Taylor, P.G. The preparation of hexasilsesquioxane (T6) cages by "Non Aqueous" Hydrolysis of trichlorosilanes. *Chem. Commun.* **2003**, *12*, 1382–1383. [CrossRef]
31. Yoshikawa, M.; Wakabayashi, R.; Tamai, M.; Kuroda, K. Synthesis of a multifunctional alkoxysiloxane oligomer. *New J. Chem.* **2014**, *38*, 5362–5368. [CrossRef]
32. Clark, J.C.; Barnes, C.E. Reaction of the $Si_8O_{20}(SnMe_3)_8$ Building Block with Silyl Chlorides: A New Synthetic Methodology for Preparing Nanostructured Building Block Solids. *Chem. Mater.* **2007**, *19*, 3212–3218. [CrossRef]
33. Lee, M.Y.; Jiao, J.; Mayes, R.; Hagaman, E.; Barnes, C.E. The targeted synthesis of single site vanadyl species on the surface and in the framework of silicate building block materials. *Catal. Today* **2011**, *160*, 153–164. [CrossRef]
34. Leskelä, M.; Ritala, M. Atomic Layer Deposition Chemistry: Recent Developments and Future Challenges. *Angew. Chem. Int. Ed.* **2003**, *42*, 5548–5554. [CrossRef] [PubMed]
35. Clavel, G.; Rauwel, E.; Willinger, M.-G.; Pinna, N. Non-aqueous sol–gel routes applied to atomic layer deposition of oxides. *J. Mater. Chem.* **2009**, *19*, 454–462. [CrossRef]
36. Lourenço, M.A.O.; Silva, R.M.; Silva, R.F.; Pinna, N.; Pronier, S.; Pires, J.; Gomes, J.R.B.; Pinto, M.L.; Ferreira, P. Turning periodic mesoporous organosilicas selective to CO_2/CH_4 separation: deposition of aluminium oxide by atomic layer deposition. *J. Mater. Chem. A* **2015**, *3*, 22860–22867. [CrossRef]
37. Arnal, P.; Corriu, R.J.P.; Leclercq, D.; Mutin, H.P.; Vioux, A. A Solution Chemistry Study of Nonhydrolytic Sol-Gel Routes to Titania. *Chem. Mater.* **1997**, *9*, 694–698. [CrossRef]
38. Styskalik, A.; Skoda, D.; Pinkas, J.; Mathur, S. Non-hydrolytic synthesis of titanosilicate xerogels by acetamide elimination and their use as epoxidation catalysts. *J. Sol-Gel Sci. Technol.* **2012**, *63*, 463–472. [CrossRef]
39. Styskalik, A.; Skoda, D.; Moravec, Z.; Abbott, J.G.; Barnes, C.E.; Pinkas, J. Synthesis of homogeneous silicophosphate xerogels by non-hydrolytic condensation reactions. *Microporous Mesoporous Mater.* **2014**, *197*, 204–212. [CrossRef]
40. Bilecka, I.; Elser, P.; Niederberger, M. Kinetic and thermodynamic aspects in the microwave-assisted synthesis of ZnO nanoparticles in benzyl alcohol. *ACS Nano* **2009**, *3*, 467–477. [CrossRef] [PubMed]
41. Kriesel, J.W.; Sander, M.S.; Tilley, T.D. Block Copolymer-Assisted Synthesis of Mesoporous, Multicomponent Oxides by Nonhydrolytic, Thermolytic Decomposition of Molecular Precursors in Nonpolar Media. *Chem. Mater.* **2001**, *13*, 3554–3563. [CrossRef]
42. Bradley, D.C.; Thomas, I.M. Organosilyloxy-derivatives of metals. Part I. Alkylsilyloxy-derivatives of titanium, zirconium, niobium, and tantalum. *J. Chem. Soc.* **1959**, 3404–3411. [CrossRef]
43. Caruso, J.; Hampden-Smith, M.J. Ester Elimination: A General Solvent Dependent Non-Hydrolytic Route to Metal and Mixed-Metal Oxides. *J. Sol-Gel Sci. Technol.* **1997**, *39*, 35–39. [CrossRef]
44. Caruso, J.; Hampden-Smith, M.J.; Duesler, E.N. Solvent Dependent Ester Elimination Reactions in the Preparation of Mixed-metal 0xo Clusters: The Synthesis of $PbSn_2(\mu_3\text{-}O)(OBut)_4(OAc)_4$. *J. Chem. Soc. Chem. Commun.* **1995**, *2*, 1041–1042. [CrossRef]
45. Jansen, M.; Guenther, E. Oxide Gels and Ceramics Prepared by a Nonhydrolytic Sol-Gel Process. *Chem. Mater.* **1995**, *7*, 2110–2114. [CrossRef]
46. Iwasaki, M.; Yasumori, A.; Shibata, S.; Yamane, M. Preparation of high homogeneity $BaO\text{-}TiO_2\text{-}SiO_2$ gel. *J. Sol-Gel Sci. Technol.* **1994**, *2*, 387–391. [CrossRef]
47. Styskalik, A.; Skoda, D.; Moravec, Z.; Babiak, M.; Barnes, C.E.; Pinkas, J. Control of micro/mesoporosity in non-hydrolytic hybrid silicophosphate xerogels. *J. Mater. Chem. A* **2015**, *3*, 7477–7487. [CrossRef]
48. Skoda, D.; Styskalik, A.; Moravec, Z.; Bezdicka, P.; Barnes, C.E.; Pinkas, J. Mesoporous titanosilicates by templated non-hydrolytic sol–gel reactions. *J. Sol-Gel Sci. Technol.* **2015**, *74*, 810–822. [CrossRef]
49. Skoda, D.; Styskalik, A.; Moravec, Z.; Bezdicka, P.; Bursik, J.; Mutin, P.H.; Pinkas, J. Mesoporous $SnO_2\text{-}SiO_2$ and Sn-silica-carbon nanocomposites by novel non-hydrolytic templated sol–gel synthesis. *RSC Adv.* **2016**, *6*, 68739–68747. [CrossRef]
50. Skoda, D.; Styskalik, A.; Moravec, Z.; Bezdicka, P.; Pinkas, J. Templated non-hydrolytic synthesis of mesoporous zirconium silicates and their catalytic properties. *J. Mater. Sci.* **2015**, *50*, 3371–3382. [CrossRef]

51. Skoda, D.; Styskalik, A.; Moravec, Z.; Bezdicka, P.; Babiak, M.; Klementova, M.; Barnes, C.E.; Pinkas, J. Novel non-hydrolytic templated sol-gel synthesis of mesoporous aluminosilicates and their use as aminolysis catalysts. *RSC Adv.* **2016**, *6*, 24273–24284. [CrossRef]
52. Chojnowski, J.; Rubinsztajn, S.; Cella, J.A.; Fortuniak, W.; Cypryk, M.; Kurjata, J.; Kaźmierski, K. Mechanism of the $B(C_6F_5)_3$-Catalyzed Reaction of Silyl Hydrides with Alkoxysilanes. Kinetic and Spectroscopic Studies. *Organometallics* **2005**, *24*, 6077–6084. [CrossRef]
53. Kurjata, J.; Fortuniak, W.; Rubinsztajn, S.; Chojnowski, J. $B(C_6F_5)_3$ catalyzed dehydrocarbon polycondensation of $PhSiH_3$ with $(MeO)_4Si$ as model polyfunctional comonomers in new route to hydrophobic silicone TQ resins. *Eur. Polym. J.* **2009**, *45*, 3372–3379. [CrossRef]
54. Rubinsztajn, S. New Facile Process for Synthesis of Borosiloxane Resins. *J. Inorg. Organomet. Polym. Mater.* **2014**, *24*, 1092–1095. [CrossRef]
55. Bradley, D.C.; Chakravarti, B.N.; Chatterjee, A.K.; Wardlaw, W.; Whitley, A. Niobium and tantalum mixed alkoxides. *J. Chem. Soc.* **1958**, 99–101. [CrossRef]
56. Pazik, R.; Tekoriute, R.; Håkansson, S.; Wiglusz, R.; Strek, W.; Seisenbaeva, G.A.; Gun'ko, Y.K.; Kessler, V.G. Precursor and solvent effects in the nonhydrolytic synthesis of complex oxide nanoparticles for bioimaging applications by the ether elimination (Bradley) reaction. *Chem. Eur. J.* **2009**, *15*, 6820–6826. [CrossRef] [PubMed]
57. Wei, H.; Lin, J.; Huang, W.; Feng, Z.; Li, D. Preparation of TeO2 based thin films by nonhydrolytic sol-gel process. *Mater. Sci. Eng. B* **2009**, *164*, 51–59. [CrossRef]
58. Corriu, R.J.P.; Leclercq, D.; Lefèvre, P.; Mutin, P.H.; Vioux, A. Preparation of monolithic metal oxide gels by a non-hydrolytic sol-gel process. *J. Mater. Chem.* **1992**, *2*, 673–674. [CrossRef]
59. Andrianainarivelo, M.; Corriu, R.J.P.; Leclercq, D.; Mutin, P.; Vioux, A. Nonhydrolytic sol-gel process: Aluminum titanate gels. *Chem. Mater.* **1997**, *9*, 1098–1102. [CrossRef]
60. Wei, H.-Y.; Jiang, W.-H.; Lin, J.; Feng, G.; Feng, Z.-B. Comparative Research on the Synthesis of Aluminum Titanate Powders by Nonhydrolytic and Hydrolytic Sol-gel Method. *J. Inorg. Mater.* **2009**, *24*, 199–203. [CrossRef]
61. Andrianainarivelo, M.; Corriu, R.J.P.; Leclercq, D.; Mutin, P.H.; Vioux, A. Non-hydrolytic sol-gel process: Zirconium titanate gels. *J. Mater. Chem.* **1997**, *7*, 279–284. [CrossRef]
62. Young, L.; Alvarez, P.T.; Liu, H.; Lind, C. Extremely Low Temperature Crystallization in the $A_2M_3O_{12}$ Family of Negative Thermal Expansion Materials. *Eur. J. Inorg. Chem.* **2016**, *2016*, 1251–1256. [CrossRef]
63. Truitt, R.; Hermes, I.; Main, A.; Sendecki, A.; Lind, C. Low Temperature Synthesis and Characterization of $AlScMo_3O_{12}$. *Materials* **2015**, *8*, 700–716. [CrossRef]
64. Gates, S.D.; Lind, C. Polymorphism in yttrium molybdate $Y_2Mo_3O_{12}$. *J. Solid State Chem.* **2007**, *180*, 3510–3514. [CrossRef]
65. Gates, S.D.; Colin, J.A.; Lind, C. Non-hydrolytic sol–gel synthesis, properties, and high-pressure behavior of gallium molybdate. *J. Mater. Chem.* **2006**, *16*, 4214–4219. [CrossRef]
66. Acosta, S.; Corriu, R.; Leclercq, D.; Mutin, P.H.; Vioux, A. Novel Non-Hydrolytic Sol-Gel Route to Metal Oxides. *J. Sol-Gel Sci. Technol.* **1994**, *2*, 25–28. [CrossRef]
67. Andrianainarivelo, M.; Corriu, R.; Leclercq, D.; Mutin, P.H.; Vioux, A. Mixed oxides SiO_2–ZrO_2 and SiO_2–TiO_2 by a non-hydrolytic sol-gel route. *J. Mater. Chem.* **1996**, *6*, 1665–1671. [CrossRef]
68. Evans, D.L. Glass structure: The bridge between the molten and crystalline states. *J. Non-Cryst. Solids* **1982**, *52*, 115–128. [CrossRef]
69. Crouzet, L.; Leclercq, D.; Mutin, P.H.; Vioux, A. Organic–inorganic materials by nonhydrolytic sol-gel processes: Organosilsesquioxane-metal oxide hybrids. *J. Sol-Gel Sci. Technol.* **2003**, *26*, 335–338. [CrossRef]
70. Lorret, O.; Lafond, V.; Mutin, P.H.; Vioux, A. One-Step Synthesis of Mesoporous Hybrid Titania−Silica Xerogels for the Epoxidation of Alkenes. *Chem. Mater.* **2006**, *18*, 4707–4709. [CrossRef]
71. Arnal, P.; Corriu, R.J.P.; Leclercq, D.; Mutin, P.H.; Vioux, A. Preparation of anatase, brookite and rutile at low temperature by non-hydrolytic sol-gel methods. *J. Mater. Chem.* **1996**, *6*, 1925–1932. [CrossRef]
72. Joo, J.; Yu, T.; Kim, Y.W.; Park, H.M.; Wu, F.; Zhang, J.Z.; Hyeon, T. Multigram Scale Synthesis and Characterization of Monodisperse Tetragonal Zirconia Nanocrystals. *J. Am. Chem. Soc.* **2003**, *125*, 6553–6557. [CrossRef] [PubMed]
73. Depner, S.W.; Kort, K.R.; Jaye, C.; Fischer, D.A.; Banerjee, S. Nonhydrolytic Synthesis and Electronic Structure of Ligand-Capped $CeO_{2-\delta}$ and CeOCl Nanocrystals. *J. Phys. Chem. C* **2009**, *113*, 14126–14134. [CrossRef]

74. Depner, S.W.; Cultrara, N.D.; Farley, K.E.; Qin, Y.; Banerjee, S. Ferroelastic Domain Organization and Precursor Control of Size in Solution-Grown Hafnium Dioxide Nanorods. *ACS Nano* **2014**, *8*, 4678–4688. [CrossRef] [PubMed]
75. Tang, J.; Fabbri, J.; Robinson, R.D.; Zhu, Y.; Herman, I.P.; Steigerwald, M.L.; Brus, L.E. Solid-Solution Nanoparticles: Use of a Nonhydrolytic Sol-Gel Synthesis To Prepare HfO_2 and $Hf_xZr_{1-x}O_2$ Nanocrystals. *Chem. Mater.* **2004**, *16*, 1336–1342. [CrossRef]
76. Trentler, T.J.; Denler, T.E.; Bertone, J.F.; Agrawal, A.; Colvin, V.L. Synthesis of TiO_2 Nanocrystals by Nonhydrolytic Solution-Based Reactions. *J. Am. Chem. Soc.* **1999**, *121*, 1613–1614. [CrossRef]
77. Goto, Y.; Omata, T.; Otsuka-Yao-Matsuo, S. Extremely Suppressed Grain Growth of Y_2O_3-Stabilized Zirconia Nanocrystals Synthesized by the Nonhydrolytic Sol-Gel Technique. *J. Electrochem. Soc.* **2009**, *156*, K4–K9. [CrossRef]
78. Bourget, L.; Mutin, P.H.; Vioux, A.; Frances, J.M. Nonhydrolytic Synthesis and Structural Study of Methoxyl-Terminated Polysiloxane D/Q Resins. *J. Polym. Sci. Part A Polym. Chem.* **1998**, *36*, 2415–2425. [CrossRef]
79. Lafond, V.; Mutin, P.H.; Vioux, A. Control of the Texture of Titania-Silica Mixed Oxides Prepared by Nonhydrolytic Sol-Gel. *Chem. Mater.* **2004**, *16*, 5380–5386. [CrossRef]
80. Acosta, S.; Corriu, R.J.P.; Leclercq, D.; Lefèvre, P.; Mutin, P.H.; Vioux, A. Preparation of Alumina gels by a non-hydrolytic sol-gel processing method. *J. Non-Cryst. Solids* **1994**, *170*, 234–242. [CrossRef]
81. Shoyama, M.; Matsumoto, N.; Hashimoto, T.; Nasu, H.; Kamiya, K. Sol-gel synthesis of zircon-effect of addition of lithium ions. *J. Mater. Sci.* **1998**, *33*, 4821–4828. [CrossRef]
82. Veytizou, C.; Quinson, J.-F.; Douy, A. Sol-gel synthesis via an aqueous semi-alkoxide route and characterization of zircon powders. *J. Mater. Chem.* **2000**, *10*, 365–370. [CrossRef]
83. Parcianello, G.; Bernardo, E.; Colombo, P. Low temperature synthesis of zircon from silicone resins and oxide nano-sized particles. *J. Eur. Ceram. Soc.* **2012**, *32*, 2819–2824. [CrossRef]
84. Sanchez, C.; Livage, J.; Henry, M.; Babonneau, F. Chemical modification of alkoxide precursors. *J. Non-Cryst. Solids* **1988**, *100*, 65–76. [CrossRef]
85. Ghosh, N.N.; Clark, J.C.; Eldridge, G.T.; Barnes, C.E. Building block syntheses of site-isolated vanadyl groups in silicate oxides. *Chem. Commun.* **2004**, 856–857. [CrossRef] [PubMed]
86. Barnes, C.E.; Sharp, K.; Albert, A.A.; Peretich, M.E.; Fulvio, P. Metal-silicate catalysts: Single site, mesoporous systems without templates. *J. Nanosci. Lett.* **2015**, *4*, 107.
87. Caruso, J.; Hampden-Smith, M.J.; Rheingold, A.L.; Yap, G. Ester Elimination Versus Ligand Exchange: The Role of the Solvent in Tin-Oxo Cluster-building Reactions. *J. Chem. Soc. Chem. Commun.* **1995**, *49*, 157–158. [CrossRef]
88. Caruso, J.; Roger, C.; Schwertfeger, F.; Hampden-Smith, M.J.; Rheingold, A.L.; Yap, G. Solvent-Dependent Ester Elimination and Ligand Exchange Reactions between Trimethylsilyl Acetate and Tin(IV) Tetra-tert-Butoxide. *Inorg. Chem.* **1995**, *34*, 449–453. [CrossRef]
89. Fujiwara, M.; Wessel, H.; Park, H.S.; Roesky, H.W. A sol-gel method using tetraethoxysilane and acetic anhydride: Immobilization of cubic μ-oxo Si-Ti complex in a silica matrix. *Chem. Mater.* **2002**, *14*, 4975–4981. [CrossRef]
90. Beckett, M.A.; Rugen-Hankey, M.P.; Varma, K.S.; Varma, K.S. Trimethoxyboroxine as an "oxygen-transfer" reagent: A non-aqueous "sol-gel" route to alkali-free borosilicate glass. *Chem. Commun.* **2000**, *37*, 1499–1500. [CrossRef]
91. Beckett, M.A.; Rugen-Hankey, M.P.; Varma, K.S. Formation of borosilicate glasses from silicon alkoxides and metaborate esters in dry non-aqueous solvents. *J. Sol-Gel Sci. Technol.* **2006**, *39*, 95–101. [CrossRef]
92. Beckett, M.A.; Rugen-Hankey, M.P.; Timmis, J.L.; Varma, K.S.; Sanchez, C.; Tallon, J.; Whyman, R. Synthesis of aluminium borate-boron oxide and binary titanium-boron and zirconium-boron oxides from metal alkoxides and $(MeO)_3B_3O_3$ in non-aqueous solvents. *Dalton Trans.* **2008**, *23*, 1503–1506. [CrossRef] [PubMed]
93. Smith, R.C.; Taylor, C.J.; Roberts, J.; Campbell, S.A.; Tiner, M.; Hegde, R.; Hobbs, C.; Gladfelter, W.L. Observation of Precursor Control over Film Stoichiometry during the Chemical Vapor Deposition of Amorphous $Ti_xSi_{1-x}O_2$ Films. *Chem. Mater.* **2000**, *12*, 2822–2824. [CrossRef]
94. Styskalik, A.; Skoda, D.; Moravec, Z.; Barnes, C.E.; Pinkas, J. Surface reactivity of non-hydrolytic silicophosphate xerogels: A simple method to create Brønsted or Lewis acid sites on porous supports. *New J. Chem.* **2016**, *40*, 3705–3715. [CrossRef]

95. Styskalik, A.; Skoda, D.; Moravec, Z.; Roupcova, P.; Barnes, C.E.; Pinkas, J. Non-aqueous template-assisted synthesis of mesoporous nanocrystalline silicon orthophosphate. *RSC Adv.* **2015**, *5*, 73670–73676. [CrossRef]
96. Sharp, K.G. A two-component, non-aqueous route to silica gel. *J. Sol-Gel Sci. Technol.* **1994**, *2*, 35–41. [CrossRef]
97. Kirszensztejn, P.; Kawałko, A.; Tolińska, A.; Przekop, R. Synthesis of SiO_2–SnO_2 gels in water free conditions. *J. Porous Mater.* **2010**, *18*, 241–249. [CrossRef]
98. Martyła, A.; Olejnik, B.; Kirszensztejn, P.; Przekop, R. Influence of the method of synthesis on hydrogen adsorption properties of mesoporous binary B_2O_3/Al_2O_3 gel systems. *Int. J. Hydrog. Energy* **2011**, *36*, 8358–8364. [CrossRef]
99. Przekop, R.; Kirszensztejn, P. Porous xerogel systems B_2O_3–Al_2O_3 obtained by the sol-gel method. *J. Non-Cryst. Solids* **2014**, *402*, 128–134. [CrossRef]
100. Liu, Y.; Wang, M.J.; Li, Z.Y.; Liu, H.T.; He, P.; Li, J.H. Preparation of porous aminopropylsilsesquioxane by a nonhydrolytic sol-gel method in ionic liquid solvent. *Langmuir* **2005**, *21*, 1618–1622. [CrossRef] [PubMed]
101. Gupta, A.K.; Singh, R.K.; Chandra, S. Crystallization kinetics behavior of ionic liquid [EMIM][BF_4] confined in mesoporous silica matrices. *RSC Adv.* **2014**, *4*, 22277–22287. [CrossRef]
102. Verma, Y.L.; Gupta, A.K.; Singh, R.K.; Chandra, S. Preparation and characterisation of ionic liquid confined hybrid porous silica derived from ultrasonic assisted non-hydrolytic sol-gel process. *Microporous Mesoporous Mater.* **2014**, *195*, 143–153. [CrossRef]
103. Viau, L.; Néouze, M.-A.; Biolley, C.; Volland, S.; Brevet, D.; Gaveau, P.; Dieudonné, P.; Galarneau, A.; Vioux, A. Ionic Liquid Mediated Sol-Gel Synthesis in the Presence of Water or Formic Acid: Which Synthesis for Which Material? *Chem. Mater.* **2012**, *24*, 3128–3134. [CrossRef]
104. Néouze, M.-A.; Le Bideau, J.; Gaveau, P.; Bellayer, S.; Vioux, A. Ionogels, New Materials Arising from the Confinement of Ionic Liquids within Silica-Derived Networks. *Chem. Mater.* **2006**, *18*, 3931–3936. [CrossRef]
105. Boday, D.J.; Tolbert, S.; Keller, M.W.; Li, Z.; Wertz, J.T.; Muriithi, B.; Loy, D.A. Non-hydrolytic formation of silica and polysilsesquioxane particles from alkoxysilane monomers with formic acid in toluene/tetrahydrofuran solutions. *J. Nanopart. Res.* **2014**, *16*, 2313. [CrossRef]
106. Park, C.-S.; Mahadik, D.B.; Park, H.-H. Enhancement of the O_2 gas sensing properties of mesoporous $Sr_{0.9}La_{0.1}TiO_3$ films by increasing the pore connectivity. *RSC Adv.* **2015**, *5*, 66384–66390. [CrossRef]
107. Bau, J.A.; Li, P.; Marenco, A.J.; Trudel, S.; Olsen, B.C.; Luber, E.J.; Buriak, J.M. Nickel/iron oxide nanocrystals with a nonequilibrium phase: Controlling size, shape, and composition. *Chem. Mater.* **2014**, *26*, 4796–4804. [CrossRef]
108. Joo, J.; Kwon, S.G.; Yu, T.; Cho, M.; Lee, J.; Yoon, J. Large-Scale Synthesis of TiO_2 Nanorods via Nonhydrolytic Sol-Gel Ester Elimination Reaction and Their Application to Photocatalytic Inactivation of *E. coli*. *J. Phys. Chem.* **2005**, *109*, 15297–15302. [CrossRef] [PubMed]
109. Sliem, M.A.; Schmidt, D.A.; Bétard, A.; Kalidindi, S.B.; Gross, S.; Havenith, M.; Devi, A.; Fischer, R.A. Surfactant-induced nonhydrolytic synthesis of phase-pure ZrO_2 nanoparticles from metal-organic and oxocluster precursors. *Chem. Mater.* **2012**, *24*, 4274–4282. [CrossRef]
110. Kejik, M.; Moravec, Z.; Barnes, C.E.; Pinkas, J. Hybrid microporous and mesoporous organosilicate covalent polymers with high porosity. *Microporous Mesoporous Mater.* **2017**, *240*, 205–215. [CrossRef]
111. Wakabayashi, R.; Kuroda, K. Siloxane-bond formation promoted by lewis acids: A nonhydrolytic sol-gel process and the piers-rubinsztajn reaction. *ChemPlusChem* **2013**, *78*, 764–774. [CrossRef]
112. Bourget, L.; Leclercq, D.; Vioux, A. Catalyzed nonhydrolytic sol-gel route to organosilsesquioxane gels. *J. Sol-Gel Sci. Technol.* **1999**, *14*, 137–147. [CrossRef]
113. Hay, J.N.; Porter, D.; Raval, H.M. A versatile route to organically-modified silicas and porous silicas via the non-hydrolytic sol-gel process. *J. Mater. Chem.* **2000**, *10*, 1811–1818. [CrossRef]
114. Apperley, D.; Hay, J.N.; Raval, H.M. Silica-dimethylsiloxane hybrids-non-hydrolytic sol-gel synthesis and characterization by NMR spectroscopy. *Chem. Mater.* **2002**, *14*, 983–988. [CrossRef]
115. Hay, J.; Raval, H.; Porter, D. A non-hydrolytic route to organically-modified silica. *Chem. Commun.* **1999**, *1*, 81–82. [CrossRef]
116. Wakabayashi, R.; Tamai, M.; Kawahara, K.; Tachibana, H.; Imamura, Y.; Nakai, H.; Kuroda, K. Direct alkoxysilylation of alkoxysilanes for the synthesis of explicit alkoxysiloxane oligomers. *J. Organomet. Chem.* **2012**, *716*, 26–31. [CrossRef]
117. Saito, S.; Yamasue, N.; Wada, H.; Shimojima, A.; Kuroda, K. Cubic Siloxanes with Both Si−H and Si−OtBu Groups for Site-Selective Siloxane Bond Formation. *Chem. Eur. J.* **2016**, *22*, 13857–13864. [CrossRef] [PubMed]

118. Kawahara, K.; Hagiwara, Y.; Kuroda, K. Dendritic, Nanosized Building Block for Siloxane-Based Materials: A Spherosilicate Dendrimer. *Chem. Eur. J.* **2011**, *17*, 13188–13196. [CrossRef] [PubMed]
119. Kuroda, K.; Shimojima, A.; Kawahara, K.; Wakabayashi, R.; Tamura, Y.; Asakura, Y.; Kitahara, M. Utilization of Alkoxysilyl Groups for the Creation of Structurally Controlled Siloxane-Based Nanomaterials. *Chem. Mater.* **2014**, *26*, 211–220. [CrossRef]
120. Arkhireeva, A.; Hay, J.N.; Manzano, M. Preparation of silsesquioxane particles via a nonhydrolytic sol-gel route. *Chem. Mater.* **2005**, *17*, 875–880. [CrossRef]
121. Jaumann, M.; Rebrov, E.A.; Kazakova, V.V.; Muzafarov, A.M.; Goedel, W.A.; Möller, M. Hyperbranched Polyalkoxysiloxanes via AB_3-Type Monomers. *Macromol. Chem. Phys.* **2003**, *204*, 1014–1026. [CrossRef]
122. Zhu, X.; Jaumann, M.; Peter, K.; Möller, M.; Melian, C.; Adams-Buda, A.; Demco, D.E.; Blümich, B. One-pot synthesis of hyperbranched polyethoxysiloxanes. *Macromolecules* **2006**, *39*, 1701–1708. [CrossRef]
123. McNamee, C.E.; Jaumann, M.; Möller, M.; Ding, A.; Hemeltjen, S.; Ebert, S.; Baumann, W.; Goedel, W.A. Formation of a Freely Suspended Membrane via a Combination of Interfacial Reaction and Wetting. *Langmuir* **2005**, *21*, 10475–10480. [CrossRef] [PubMed]
124. Wang, H.; Zhu, X.; Tsarkova, L.; Pich, A.; Möller, M. All-Silica Colloidosomes with a Particle-Bilayer Shell. *ACS Nano* **2011**, *5*, 3937–3942. [CrossRef] [PubMed]
125. Wang, H.; Agrawal, G.; Tsarkova, L.; Zhu, X.; Möller, M. Self-Templating Amphiphilic Polymer Precursors for Fabricating Mesostructured Silica Particles: A Water-Based Facile and Universal Method. *Adv. Mater.* **2013**, *25*, 1017–1021. [CrossRef] [PubMed]
126. Zhang, K.; An, J.; Su, Y.; Zhang, J.; Wang, Z.; Cheng, T.; Liu, G. Amphiphilic Hyperbranched Polyethoxysiloxane: A Self-Templating Assembled Platform to Fabricate Functionalized Mesostructured Silicas for Aqueous Enantioselective Reactions. *ACS Catal.* **2016**, *6*, 6229–6235. [CrossRef]
127. Grande, J.B.; Urlich, T.; Dickie, T.; Brook, M.A. Silicone dendrons and dendrimers from orthogonal SiH coupling reactions. *Polym. Chem.* **2014**, *5*, 6728–6739. [CrossRef]
128. Rubinsztajn, S.; Cella, J.A. A new polycondensation process for the preparation of polysiloxane copolymers. *Macromolecules* **2005**, *38*, 1061–1063. [CrossRef]
129. Grande, J.B.; Fawcett, A.S.; McLaughlin, A.J.; Gonzaga, F.; Bender, T.P.; Brook, M.A. Anhydrous formation of foamed silicone elastomers using the Piers-Rubinsztajn reaction. *Polymer* **2012**, *53*, 3135–3142. [CrossRef]
130. Chojnowski, J.; Rubinsztajn, S.; Fortuniak, W.; Kurjata, J. Synthesis of Highly Branched Alkoxysiloxane-Dimethylsiloxane Copolymers by Nonhydrolytic Dehydrocarbon Polycondensation Catalyzed by *Tris*(pentafluorophenyl)borane. *Macromolecules* **2008**, *41*, 7352–7358. [CrossRef]
131. Pan, D.; Yi, E.; Doan, P.H.; Furgal, J.C.; Schwartz, M.; Clark, S.; Goodson Iii, T.; Laine, R.M. Microporous inorganic/organic hybrids via oxysilylation of a cubic symmetry nanobuilding block $[(HMe_2SiOSiO_{1.5})_8]$ with $R_xSi(OEt)_{4-x}$. *J. Ceram. Soc. Jpn.* **2015**, *123*, 756–763. [CrossRef]
132. Nassar, E.J.; Dos Santos Pereira, P.F.; De Oliveira Nassor, E.C.; Ávila, L.R.; Ciuffi, K.J.; Calefi, P.S. Nonhydrolytic sol-gel synthesis and characterization of YAG. *J. Mater. Sci.* **2007**, *42*, 2244–2249. [CrossRef]
133. Pereira, P.F.S.; Matos, M.G.; Ferreira, C.M.A.; De Faria, E.H.; Calefi, P.S.; Rocha, L.A.; Ciuffi, K.J.; Nassar, E.J. Aluminate matrix doped with $Tm^{3+}/Tb^{3+}/Eu^{3+}$ obtained by non-hydrolytic sol-gel route: White light emission. *J. Lumin.* **2014**, *146*, 394–397. [CrossRef]
134. Matos, M.G.; De Faria, E.H.; Rocha, L.A.; Calefi, P.S.; Ciuffi, K.J.; Nassar, E.J.; Sarmento, V.H.V. Synthesis and photoluminescent properties of yttrium vanadate phosphor prepared by the non-hydrolytic sol-gel process. *J. Lumin.* **2014**, *147*, 190–195. [CrossRef]
135. Matos, M.G.; Pereira, P.F.S.; Calefi, P.S.; Ciuffi, K.J.; Nassar, E.J. Preparation of a $GdCaAl_3O_7$ matrix by the non-hydrolytic sol-gel route. *J. Lumin.* **2009**, *129*, 1120–1124. [CrossRef]
136. Mokhothu, T.H.; Luyt, A.S.; Messori, M. Preparation and characterization of EPDM/silica nanocomposites prepared through non-hydrolytic sol-gel method in the absence and presence of a coupling agent. *Express Polym. Lett.* **2014**, *8*, 809–822. [CrossRef]
137. Nassar, E.J.; Avila, L.R.; Pereira, P.F.S.; Mello, C.; De Lima, O.J.; Ciuffi, K.J.; Carlos, L.D. Eu(III) incorporation in sol-gel aluminum-yttrium matrix by non-hydrolytic route. *J. Lumin.* **2005**, *111*, 159–166. [CrossRef]
138. Orsini, G.; Tricoli, V. Facile nonhydrolytic sol-gel route to mesoporous mixed-conducting tungsten oxide. *J. Mater. Chem.* **2011**, *21*, 14530–14542. [CrossRef]

139. Pereira, P.F.S.; Matos, M.G.; Ávila, L.R.; Nassor, E.C.O.; Cestari, A.; Ciuffi, K.J.; Calefi, P.S.; Nassar, E.J. Red, green and blue (RGB) emission doped $Y_3Al_5O_{12}$ (YAG) phosphors prepared by non-hydrolytic sol-gel route. *J. Lumin.* **2010**, *130*, 488–493. [CrossRef]
140. Silva, G.M.; De Faria, E.H.; Nassar, E.J.; Ciuffi, K.J.; Calefi, P.S. Synthesis of Indium Tin Oxide Nanoparticles by a Nonhydrolytic Sol-Gel Method. *Quim. Nova* **2012**, *35*, 473–476. [CrossRef]
141. Yoo, Y.B.; Park, J.H.; Song, K.M.; Lee, S.J.; Baik, H.K. Non-hydrolytic ester-elimination reaction and its application in solution-processed zinc tin oxide thin film transistors. *J. Sol-Gel Sci. Technol.* **2012**, *64*, 257–263. [CrossRef]
142. Hamden, Z.; Bouattour, S.; Ferraria, A.M.; Ferreira, D.P.; Vieira Ferreira, L.F.; Botelho do Rego, A.M.; Boufi, S. In situ generation of TiO_2 nanoparticles using chitosan as a template and their photocatalytic activity. *J. Photochem. Photobiol. A Chem.* **2016**, *321*, 211–222. [CrossRef]
143. Choi, K.M.; Wakabayashi, R.; Tatsumi, T.; Yokoi, T.; Kuroda, K. Usefulness of alkoxyltitanosiloxane for the preparation of mesoporous silica containing a large amount of isolated titanium. *J. Colloid Interface Sci.* **2011**, *359*, 240–247. [CrossRef] [PubMed]
144. Bassindale, A.R.; Gentle, T. Derivatisation of octasilsesquioxane with alcohols and silanols. *J. Organomet. Chem.* **1996**, *521*, 391–393. [CrossRef]
145. Wada, Y.; Iyoki, K.; Sugawara-Narutaki, A.; Okubo, T.; Shimojima, A. Diol-linked microporous networks of cubic siloxane cages. *Chem. Eur. J.* **2013**, *19*, 1700–1705. [CrossRef] [PubMed]
146. Moravec, Z.; Sluka, R.; Necas, M.; Jancik, V.; Pinkas, J. A structurally diverse series of aluminum chloride alkoxides $[Cl_xAl(\mu\text{-}OR)_y]_n$ (R = ^{n}Bu, ^{c}Hex, Ph, 2,4-^{t}Bu$_2$C$_6$H$_3$). *Inorg. Chem.* **2009**, *48*, 8106–8114. [CrossRef] [PubMed]
147. Kitschke, P.; Schulze, S.; Hietschold, M.; Mehring, M. Synthesis of germanium dioxide nanoparticles in benzyl alcohol—A comparison. *Main Group Met. Chem.* **2013**, *36*, 209–214. [CrossRef]
148. Niederberger, M.; Garnweitner, G.; Pinna, N.; Antonietti, M. Nonaqueous and Halide-Free Route to Crystalline $BaTiO_3$, $SrTiO_3$, and (Ba,Sr)TiO_3 Nanoparticles via a Mechanism Involving C−C Bond Formation. *J. Am. Chem. Soc.* **2004**, *126*, 9120–9126. [CrossRef] [PubMed]
149. Pinna, N.; Antonietti, M.; Niederberger, M. A novel nonaqueous route to V_2O_3 and Nb_2O_5 nanocrystals. *Colloids Surf. A* **2004**, *250*, 211–213. [CrossRef]
150. Pinna, N.; Garnweitner, G.; Beato, P.; Niederberger, M.; Antonietti, M. Synthesis of Yttria-Based Crystalline and Lamellar Nanostructures and their Formation Mechanism. *Small* **2004**, *1*, 112–121. [CrossRef] [PubMed]
151. Bilecka, I.; Luo, L.; Djerdj, I.; Rossell, M.D.; Jagodič, M.; Jagličić, Z.; Masubuchi, Y.; Kikkawa, S.; Niederberger, M. Microwave-Assisted Nonaqueous Sol-Gel Chemistry for Highly Concentrated ZnO-Based Magnetic Semiconductor Nanocrystals. *J. Phys. Chem. C* **2011**, *115*, 1484–1495. [CrossRef]
152. Luo, L.; Bozyigit, D.; Wood, V.; Niederberger, M. High-quality transparent electrodes spin-cast from preformed antimony-doped tin oxide nanocrystals for thin film optoelectronics. *Chem. Mater.* **2013**, *25*, 4901–4907. [CrossRef]
153. Bilecka, I.; Hintennach, A.; Djerdj, I.; Novák, P.; Niederberger, M. Efficient microwave-assisted synthesis of $LiFePO_4$ mesocrystals with high cycling stability. *J. Mater. Chem.* **2009**, *19*, 5125–5128. [CrossRef]
154. Bilecka, I.; Hintennach, A.; Rossell, M.D.; Xie, D.; Novák, P.; Niederberger, M. Microwave-assisted solution synthesis of doped $LiFePO_4$ with high specific charge and outstanding cycling performance. *J. Mater. Chem.* **2011**, *21*, 5881–5890. [CrossRef]
155. Morselli, D.; Niederberger, M.; Bilecka, I.; Bondioli, F. Double role of polyethylene glycol in the microwaves-assisted non-hydrolytic synthesis of nanometric TiO_2: Oxygen source and stabilizing agent. *J. Nanopart. Res.* **2014**, *16*, 4519–4521. [CrossRef]
156. Ito, D.; Yokoyama, S.; Zaikova, T.; Masuko, K.; Hutchison, J.E. Synthesis of ligand-stabilized metal oxide nanocrystals and epitaxial core/shell nanocrystals via a lower-temperature esterification process. *ACS Nano* **2014**, *8*, 64–75. [CrossRef] [PubMed]
157. Bradley, D.C.; Chakravarti, B.N.; Wardlaw, W. Structural chemistry of the alkoxides. Part VIII. Isomeric butoxides and pentyloxides of niobium. *J. Chem. Soc.* **1956**, 4439–4442. [CrossRef]
158. Turova, N.Y.; Kessler, V.G.; Kucheiko, S.I. Molybdenum and tungsten (VI) bimetallic alkoxides. Decomposition accompanied by dialkylether elimination. *Polyhedron* **1991**, *10*, 2617–2628. [CrossRef]
159. Senouci, A.; Yaakoub, M.; Huguenard, C.; Henry, M. Molecular templating using titanium(iv)(oxo)alkoxides and titanium(iv)(oxo)aryloxides. *J. Mater. Chem.* **2004**, *14*, 3215–3230. [CrossRef]

160. Kessler, V.G.; Turova, N.Y.; Panov, A.N.; Starikova, Z.A.; Yanovsky, A.I.; Struchkov, Y.T.; Benlian, D. Synthesis, crystal and molecular structure of a new heterometallic oxo-2-methoxyethoxide, $BaMo_2O_5(OC_2H_4OMe)_4(HOC_2H_4OMe)$. *Polyhedron* **1998**, *17*, 4189–4193. [CrossRef]
161. Laye, R.H.; McInnes, E.J.L. Solvothermal Synthesis of Paramagnetic Molecular Clusters. *Eur. J. Inorg. Chem.* **2004**, *2004*, 2811–2818. [CrossRef]
162. Pazik, R.; Seisenbaeva, G.A.; Gohil, S.; Wiglusz, R.; Kępiński, L.; Strek, W.; Kessler, V.G. Simple and efficient synthesis of a Nd:$LaAlO_3$ NIR nanophosphor from rare earth alkoxo-monoaluminates $Ln_2Al_2(O^iPr)_{12}(^iPrOH)_2$ single source precursors by Bradley reaction. *Inorg. Chem.* **2010**, *49*, 2684–2691. [CrossRef] [PubMed]
163. Abtmeyer, S.; Pązik, R.; Wiglusz, R.J.; Małecka, M.; Seisenbaeva, G.A.; Kessler, V.G. Lanthanum Molybdate Nanoparticles from the Bradley Reaction: Factors Influencing Their Composition, Structure, and Functional Characteristics as Potential Matrixes for Luminescent Phosphors. *Inorg. Chem.* **2014**, *53*, 943–951. [CrossRef] [PubMed]
164. Kessler, V.G.; Nikitin, K.V.; Belokon, A.I. A new argument in favor of the ether elimination mechanism: Formation of acetals on action of molybdenum alkoxides on carbonyl compounds. *Polyhedron* **1998**, *17*, 2309–2311. [CrossRef]
165. Pązik, R.; Piasecka, E.; Małecka, M.; Kessler, V.G.; Idzikowski, B.; Śniadecki, Z.; Wiglusz, R.J. Facile non-hydrolytic synthesis of highly water dispersible, surfactant free nanoparticles of synthetic MFe_2O_4 (M–Mn^{2+}, Fe^{2+}, Co^{2+}, Ni^{2+}) ferrite spinel by a modified Bradley reaction. *RSC Adv.* **2013**, *3*, 12230–12243. [CrossRef]
166. Leonhardt, C.; Brumm, S.; Seifert, A.; Cox, G.; Lange, A.; Rüffer, T.; Schaarschmidt, D.; Lang, H.; Jöhrmann, N.; Hietschold, M.; et al. Tin Oxide Nanoparticles and SnO_2/SiO_2 Hybrid Materials by Twin Polymerization Using Tin(IV) Alkoxides. *ChemPlusChem* **2013**, *78*, 1400–1412. [CrossRef]
167. Böttger-Hiller, F.; Lungwitz, R.; Seifert, A.; Hietschold, M.; Schlesinger, M.; Mehring, M.; Spange, S. Nanoscale Tungsten Trioxide Synthesized by In Situ Twin Polymerization. *Angew. Chem. Int. Ed.* **2009**, *48*, 8878–8881. [CrossRef] [PubMed]
168. Spange, S.; Grund, S. Nanostructured Organic-Inorganic Composite Materials by Twin Polymerization of Hybrid Monomers. *Adv. Mater.* **2009**, *21*, 2111–2116. [CrossRef]
169. Spange, S.; Kempe, P.; Seifert, A.; Auer, A.A.; Ecorchard, P.; Lang, H.; Falke, M.; Hietschold, M.; Pohlers, A.; Hoyer, W.; et al. Nanocomposites with Structure Domains of 0.5 to 3 nm by Polymerization of Silicon Spiro Compounds. *Angew. Chem. Int. Ed.* **2009**, *48*, 8254–8258. [CrossRef] [PubMed]
170. Mehner, A.; Rüffer, T.; Lang, H.; Pohlers, A.; Hoyer, W.; Spange, S. Synthesis of Nanosized TiO_2 by Cationic Polymerization of (μ_4-oxido)-hexakis(μ-furfuryloxo)-octakis(furfuryloxo)-tetra-titanium. *Adv. Mater.* **2008**, *20*, 4113–4117. [CrossRef]
171. Crespy, D.; Landfester, K. Making dry fertile: A practical tour of non-aqueous emulsions and miniemulsions, their preparation and some applications. *Soft Matter* **2011**, *7*, 11054–11064. [CrossRef]
172. Bagshaw, S.A.; Prouzet, E.; Pinnavaia, T.J. Templating of Mesoporous Molecular Sieves by Nonionic Polyethylene Oxide Surfactants. *Science* **1995**, *269*, 1242–1244. [CrossRef] [PubMed]
173. Yang, P.; Zhao, D.; Margolese, D.I.; Chmelka, B.F.; Stucky, G.D. Block Copolymer Templating Syntheses of Mesoporous Metal Oxides with Large Ordering Lengths and Semicrystalline Framework. *Chem. Mater.* **1999**, *11*, 2813–2826. [CrossRef]
174. Dombrowski, J.P.; Johnson, G.R.; Bell, A.T.; Tilley, T.D. $Ga[OSi(O^tBu)_3]_3\cdot THF$, a thermolytic molecular precursor for high surface area gallium-containing silica materials of controlled dispersion and stoichiometry. *Dalton Trans.* **2016**, *45*, 11025–11034. [CrossRef] [PubMed]
175. Brutchey, R.L.; Lugmair, C.G.; Schebaum, L.O.; Tilley, T.D. Thermolytic conversion of a bis(alkoxy)tris (siloxy)tantalum(V) single-source molecular precursor to catalytic tantala-silica materials. *J. Catal.* **2005**, *229*, 72–81. [CrossRef]
176. Skoda, D. 2016. Synthesis of Metallosilicate Materials by Non-Hydrolytic Methods. Ph.D. Thesis, Masarykova Univerzita, Brno, Czech Republic, 2016.
177. Bouchmella, K.; Hubert Mutin, P.; Stoyanova, M.; Poleunis, C.; Eloy, P.; Rodemerck, U.; Gaigneaux, E.M.; Debecker, D.P. Olefin metathesis with mesoporous rhenium–silicium–aluminum mixed oxides obtained via a one-step non-hydrolytic sol-gel route. *J. Catal.* **2013**, *301*, 233–241. [CrossRef]

178. Bouchmella, K.; Stoyanova, M.; Rodemerck, U.; Debecker, D.P.; Hubert Mutin, P. Avoiding rhenium loss in non-hydrolytic synthesis of highly active Re-Si-Al olefin metathesis catalysts. *Catal. Commun.* **2015**, *58*, 183–186. [CrossRef]
179. Debecker, D.P.; Bouchmella, K.; Delaigle, R.; Eloy, P.; Poleunis, C.; Bertrand, P.; Gaigneaux, E.M.; Mutin, P.H. One-step non-hydrolytic sol-gel preparation of efficient V_2O_5-TiO_2 catalysts for VOC total oxidation. *Appl. Catal. B* **2010**, *94*, 38–45. [CrossRef]
180. Debecker, D.P.; Bouchmella, K.; Stoyanova, M.; Rodemerck, U.; Gaigneaux, E.M.; Hubert Mutin, P. A non-hydrolytic sol-gel route to highly active MoO_3–SiO_2–Al_2O_3 metathesis catalysts. *Catal. Sci. Technol.* **2012**, *2*, 1157–1164. [CrossRef]
181. Debecker, D.P.; Delaigle, R.; Bouchmella, K.; Eloy, P.; Gaigneaux, E.M.; Mutin, P.H. Total oxidation of benzene and chlorobenzene with MoO_3- and WO_3-promoted V_2O_5/TiO_2 catalysts prepared by a nonhydrolytic sol-gel route. *Catal. Today* **2010**, *157*, 125–130. [CrossRef]
182. Maksasithorn, S.; Praserthdam, P.; Suriye, K.; Devillers, M.; Debecker, D.P. WO_3-based catalysts prepared by non-hydrolytic sol-gel for the production of propene by cross-metathesis of ethene and 2-butene. *Appl. Catal. A Gen.* **2014**, *488*, 200–207. [CrossRef]
183. Caetano, B.L.; Rocha, L.A.; Molina, E.; Rocha, Z.N.; Ricci, G.; Calefi, P.S.; de Lima, O.J.; Mello, C.; Nassar, E.J.; Ciuffi, K.J. Cobalt aluminum silicate complexes prepared by the non-hydrolytic sol-gel route and their catalytic activity in hydrocarbon oxidation. *Appl. Catal. A Gen.* **2006**, *311*, 122–134. [CrossRef]
184. Ricci, G.P.; Rocha, Z.N.; Nakagaki, S.; Castro, K.A.D.F.; Crotti, A.E.M.; Calefi, P.S.; Nassar, E.J.; Ciuffi, K.J. Iron-alumina materials prepared by the non-hydrolytic sol-gel route: Synthesis, characterization and application in hydrocarbons oxidation using hydrogen peroxide as oxidant. *Appl. Catal. A Gen.* **2010**, *389*, 147–154. [CrossRef]
185. Moggi, P.; Predieri, G.; Cauzzi, D.; Devillers, M.; Ruiz, P.; Morselli, S.; Ligabue, O. Sol-gel preparation of pure and silica-dispersed vanadium and niobium catalysts active in oxidative dehydrogenation of propane. In *Scientific Bases for the Preparation of Heterogeneous Catalysts*; Elsevier: Boston, MA, USA, 2000; Volume 143, pp. 149–157.
186. Matos, M.G.; Calefi, P.S.; Ciuffi, K.J.; Nassar, E.J. Synthesis and luminescent properties of gadolinium aluminates phosphors. *Inorg. Chim. Acta* **2011**, *375*, 63–69. [CrossRef]
187. Hofmann, M.; Rainer, M.; Schulze, S.; Hietschold, M.; Mehring, M. Nonaqueous Synthesis of a Bismuth Vanadate Photocatalyst By Using Microwave Heating: Photooxidation versus Photosensitized Decomposition in. *ChemCatChem* **2015**, *7*, 1357–1365. [CrossRef]
188. Baiz, T.I.; Gindhart, A.M.; Kraemer, S.K.; Lind, C. Synthesis of $MgHf(WO_4)_3$ and $MgZr(WO_4)_3$ using a non-hydrolytic sol-gel method. *J. Sol-Gel Sci. Technol.* **2008**, *47*, 128–130. [CrossRef]
189. Lind, C.; Gates, S.D.; Pedoussaut, N.M.; Baiz, T.I. Novel Materials through Non-Hydrolytic Sol-Gel Processing: Negative Thermal Expansion Oxides and Beyond. *Materials* **2010**, *3*, 2567–2587. [CrossRef]
190. Zhou, X.; Heinrich, C.P.; Kluenker, M.; Dolique, S.; Mull, D.L.; Lind, C. Non-hydrolytic sol-gel synthesis of tantalum sulfides. *J. Sol-Gel Sci. Technol.* **2014**, *69*, 596–604. [CrossRef]
191. Zhou, X.; Soldat, A.C.; Lind, C. Phase selective synthesis of copper sulfides by non-hydrolytic sol-gel methods. *RSC Adv.* **2014**, *4*, 717–726. [CrossRef]
192. Leidich, S.; Buechele, D.; Lauenstein, R.; Kluenker, M.; Lind, C. "Non-hydrolytic" sol-gel synthesis of molybdenum sulfides. *J. Solid State Chem.* **2016**, *242*, 175–181. [CrossRef]
193. Ludi, B.; Olliges-Stadler, I.; Rossell, M.D.; Niederberger, M. Extension of the benzyl alcohol route to metal sulfides: "Nonhydrolytic" thio sol-gel synthesis of ZnS and SnS_2. *Chem. Commun.* **2011**, *47*, 5280–5282. [CrossRef] [PubMed]
194. Kemnitz, E.; Noack, J. The non-aqueous fluorolytic sol-gel synthesis of nanoscaled metal fluorides. *Dalton Trans.* **2015**, *44*, 19411–19431. [CrossRef] [PubMed]
195. Livage, J.; Barboux, P.; Vandenborre, M.T.; Schmutz, C.; Taulelle, F. Sol-gel synthesis of phosphates. *J. Non-Cryst. Solids* **1992**, *147–148*, 18–23. [CrossRef]
196. Willinger, M.-G.; Clavel, G.; Di, W.; Pinna, N. A general soft-chemistry route to metal phosphate nanocrystals. *J. Ind. Eng. Chem.* **2009**, *15*, 883–887. [CrossRef]
197. Jähnigen, S.; Brendler, E.; Böhme, U.; Kroke, E. Synthesis of silicophosphates containing SiO_6-octahedra under ambient conditions-reactions of anhydrous H_3PO_4 with alkoxysilanes. *Chem. Commun.* **2012**, *48*, 7675–7677. [CrossRef] [PubMed]

198. Jähnigen, S.; Brendler, E.; Böhme, U.; Heide, G.; Kroke, E. Silicophosphates containing SiO_6 octahedra-anhydrous synthesis under ambient conditions. *New J. Chem.* **2014**, *38*, 744–751. [CrossRef]
199. Tokuda, Y.; Tanaka, Y.; Takahashi, M.; Ihara, R.; Yoko, T. Silicophosphate/Silicophosphite Hybrid Materials Prepared by Solventless Ethanol Condensation. *J. Ceram. Soc. Jpn.* **2009**, *117*, 842–846. [CrossRef]
200. Niida, H.; Tokuda, Y.; Takahashi, M.; Uchino, T.; Yoko, T. Structure of organic–inorganic hybrid low-melting glasses from ^{29}Si NMR and ab initio molecular orbital calculations. *J. Non-Cryst. Solids* **2002**, *311*, 145–153. [CrossRef]
201. Mizuno, M.; Takahashi, M.; Tokuda, Y.; Yoko, T. Organic−Inorganic Hybrid Material of Phenyl-Modified Polysilicophosphate Prepared through Nonaqueous Acid-Base Reaction. *Chem. Mater.* **2006**, *18*, 2075–2080. [CrossRef]
202. Niida, H.; Takahashi, M.; Uchino, T.; Yoko, T. Preparation and structure of organic–inorganic hybrid precursors for new type low-melting glasses. *J. Non-Cryst. Solids* **2002**, *306*, 292–299. [CrossRef]
203. Mizuno, M.; Takahashi, M.; Tokuda, Y.; Yoko, T. Substituent effect on the formation of organically-modified silicate-phosphate alternating copolymer through nonaqueous acid–base reaction. *J. Sol-Gel Sci. Technol.* **2007**, *44*, 47–52. [CrossRef]
204. Pinkas, J.; Wessel, H.; Yang, Y.; Montero, M.L.; Noltemeyer, M.; Fröba, M.; Roesky, H.W. Reactions of Phosphoric Acid Triesters with Aluminum and Gallium Amides. *Inorg. Chem.* **1998**, *37*, 2450–2457. [CrossRef]
205. Pinkas, J.; Chakraborty, D.; Yang, Y.; Murugavel, R.; Noltemeyer, M.; Roesky, H.W. Reactions of Trialkyl Phosphates with Trialkyls of Aluminum and Gallium: New Route to Alumino- and Gallophosphate Compounds via Dealkylsilylation. *Organometallics* **1999**, *18*, 523–528. [CrossRef]
206. Di Vona, M.L.; Traversa, E.; Licoccia, S. Nonhydrolytic Synthesis of NASICON of Composition $Na_3Zr_2Si_2PO_{12}$: A Spectroscopic Study. *Chem. Mater.* **2001**, *13*, 141–144. [CrossRef]
207. Corriu, R.J. P.; Leclercq, D.; Mutin, P.H.; Sarlin, L.; Vioux, A. Nonhydrolytic sol-gel routes to layered metal(IV) and silicon phosphonates. *J. Mater. Chem.* **1998**, *8*, 1827–1833. [CrossRef]
208. Grader, G.S.; Shter, G.E.; De Hazan, Y. Novel ceramic foams from crystals of $AlCl_3(Pr^i{}_2O)$ complex. *J. Mater. Res.* **1999**, *14*, 1485–1494. [CrossRef]
209. Grader, G.; Shter, G.; Dehazan, Y. Method of Producing Ceramic Foams. EP1093448 A1, 17 March 1999.
210. Kaper, H.; Bouchmella, K.; Mutin, P.H.; Goettmann, F. High-Surface-Area SiO_2-ZrO_2 Mixed Oxides as Catalysts for the Friedel-Crafts-Type Alkylation of Arenes with Alcohols and Tandem Cyclopropanation Reactions. *ChemCatChem* **2012**, *4*, 1813–1818. [CrossRef]
211. Lafond, V.; Mutin, P.H.; Vioux, A. Non-hydrolytic sol-gel routes based on alkyl halide elimination: Toward better mixed oxide catalysts and new supports: Application to the preparation of a SiO_2–TiO_2 epoxidation catalyst. *J. Mol. Catal. A Chem.* **2002**, *182–183*, 81–88. [CrossRef]
212. Cojocariu, A.M.; Mutin, P.H.; Dumitriu, E.; Aboulaich, A.; Vioux, A.; Fajula, F.; Hulea, V. Non-hydrolytic SiO_2–TiO_2 mesoporous xerogels—Efficient catalysts for the mild oxidation of sulfur organic compounds with hydrogen peroxide. *Catal. Today* **2010**, *157*, 270–274. [CrossRef]
213. Cojocariu, A.M.; Mutin, P.H.; Dumitriu, E.; Fajula, F.; Vioux, A.; Hulea, V. Mild oxidation of bulky organic compounds with hydrogen peroxide over mesoporous TiO_2-SiO_2 xerogels prepared by non-hydrolytic sol-gel. *Appl. Catal. B* **2010**, *97*, 407–413. [CrossRef]
214. Debecker, D.P.; Bouchmella, K.; Poleunis, C.; Eloy, P.; Bertrand, P.; Gaigneaux, E.M.; Mutin, P.H. Design of $SiO_2-Al_2O_3-MoO_3$ Metathesis Catalysts by Nonhydrolytic Sol-Gel. *Chem. Mater.* **2009**, *21*, 2817–2824. [CrossRef]
215. Debecker, D.P.; Stoyanova, M.; Colbeau-Justin, F.; Rodemerck, U.; Boissière, C.; Gaigneaux, E.M.; Sanchez, C. One-pot aerosol route to MoO_3–SiO_2–Al_2O_3 catalysts with ordered super microporosity and high olefin metathesis activity. *Angew. Chem. Int. Ed.* **2012**, *51*, 2129–2131. [CrossRef] [PubMed]
216. Albrbar, A.J.; Djokić, V.; Bjelajac, A.; Kovač, J.; Ćirković, J.; Mitrić, M.; Janaćković, D.; Petrović, R. Visible-light active mesoporous, nanocrystalline N,S-doped and co-doped titania photocatalysts synthesized by non-hydrolytic sol-gel route. *Ceram. Int.* **2016**, *42*, 16718–16728. [CrossRef]
217. Escamilla-Pérez, A.M.; Louvain, N.; Kaschowitz, M.; Freunberger, S.; Fontaine, O.; Boury, B.; Brun, N.; Mutin, P.H. Lithium insertion properties of mesoporous nanocrystalline TiO_2 and TiO_2–V_2O_5 microspheres prepared by non-hydrolytic sol-gel. *J. Sol-Gel Sci. Technol.* **2016**, *79*, 270–278. [CrossRef]

218. Yu, S.-H.; Pucci, A.; Herntrich, T.; Willinger, M.-G.; Baek, S.-H.; Sung, Y.-E.; Pinna, N. Surfactant-free nonaqueous synthesis of lithium titanium oxide (LTO) nanostructures for lithium ion battery applications. *J. Mater. Chem.* **2011**, *21*, 806–810. [CrossRef]
219. Baek, S.; Yu, S.-H.; Park, S.-K.; Pucci, A.; Marichy, C.; Lee, D.-C.; Sung, Y.-E.; Piao, Y.; Pinna, N. A one-pot microwave-assisted non-aqueous sol-gel approach to metal oxide/graphene nanocomposites for Li-ion batteries. *RSC Adv.* **2011**, *1*, 1687–1690. [CrossRef]
220. Yu, S.H.; Conte, D.E.; Baek, S.; Lee, D.C.; Park, S.K.; Lee, K.J.; Piao, Y.; Sung, Y.E.; Pinna, N. Structure-properties relationship in iron oxide-reduced graphene oxide nanostructures for Li-ion batteries. *Adv. Funct. Mater.* **2013**, *23*, 4293–4305. [CrossRef]
221. Caresani, J.R.; Lattuada, R.M.; Radtke, C.; Dos Santos, J.H.Z. Attempts made to heterogenize MAO via encapsulation within silica through a non-hydrolytic sol-gel process. *Powder Technol.* **2014**, *252*, 56–64. [CrossRef]
222. Fisch, A.G.; Cardozo, N.S.M.; Secchi, A.R.; Stedile, F.C.; da Silveira, N.P.; dos Santos, J.H.Z. Investigation of silica particle structure containing metallocene immobilized by a sol-gel method. *J. Non-Cryst. Solids* **2008**, *354*, 3973–3979. [CrossRef]
223. Capeletti, L.B.; Dos Santos, J.H.Z.; Moncada, E.; Da Rocha, Z.N.; Pepe, I.M. Encapsulated alizarin red species: The role of the sol-gel route on the interaction with silica matrix. *Powder Technol.* **2013**, *237*, 117–124. [CrossRef]
224. Coles, M.P.; Lugmair, C.G.; Terry, K.W.; Tilley, T.D. Titania-Silica Materials from the Molecular Precursor $Ti[OSi(O^tBu)_3]_4$: Selective Epoxidation Catalysts. *Chem. Mater.* **2000**, *12*, 122–131. [CrossRef]
225. Hutter, R.; Mallat, T.; Baiker, A. Titania Silica Mixed Oxides II. Catalytic Behavior in Olefin Epoxidation. *J. Catal.* **1995**, *153*, 177–189. [CrossRef]
226. Bertinchamps, F.; Grégoire, C.; Gaigneaux, E.M. Systematic investigation of supported transition metal oxide based formulations for the catalytic oxidative elimination of (chloro)-aromatics. *Appl. Catal. B* **2006**, *66*, 10–22. [CrossRef]
227. Green, W.H.; Le, K.P.; Grey, J.; Au, T.T.; Sailor, M.J. White Phosphors from a Silicate-Carboxylate Sol-Gel Precursor That Lack Metal Activator Ions. *Science* **1997**, *276*, 1826–1828. [CrossRef]
228. Xi, W.; Scott, T.F.; Kloxin, C.J.; Bowman, C.N. Click chemistry in materials science. *Adv. Funct. Mater.* **2014**, *24*, 2572–2590. [CrossRef]
229. Cattoën, X.; Noureddine, A.; Croissant, J.; Moitra, N.; Bürglová, K.; Hodačová, J.; De Los Cobos, O.; Lejeune, M.; Rossignol, F.; Toulemon, D.; et al. Click approaches in sol-gel chemistry. *J. Sol-Gel Sci. Technol.* **2014**, *70*, 245–253. [CrossRef]
230. Bürglová, K.; Noureddine, A.; Hodačová, J.; Toquer, G.; Cattoën, X.; Wongchiman, M. A general method for preparing bridged organosilanes with pendant functional groups and functional mesoporous organosilicas. *Chem. Eur. J.* **2014**, *20*, 10371–10382. [CrossRef] [PubMed]

© 2017 by the authors. Licensee MDPI, Basel, Switzerland. This article is an open access article distributed under the terms and conditions of the Creative Commons Attribution (CC BY) license (http://creativecommons.org/licenses/by/4.0/).